



Architecture, persistence and dissolution of a 20 to 45 year old trichloroethene DNAPL source zone



Michael O. Rivett^{a,*}, Rachel A. Dearden^{a,b}, Gary P. Wealhall^{b,c}

^a Water Sciences, School of Geography, Earth & Environmental Sciences, University of Birmingham, Birmingham B15 2TT, UK

^b British Geological Survey, Environmental Science Centre, Keyworth, Nottingham NG12 5GG, UK

^c Geosyntec Consultants, Inc., 2-130 Research Lane, Guelph, Ontario N1G 5G3, Canada

ARTICLE INFO

Article history:

Received 29 October 2013

Received in revised form 11 September 2014

Accepted 14 September 2014

Available online 28 September 2014

Keywords:

DNAPL

Chlorinated solvent

Trichloroethene

TCE

Source zone architecture

Dissolution

Groundwater

Cis-dichloroethene

ABSTRACT

A detailed field-scale investigation of processes controlling the architecture, persistence and dissolution of a 20 to 45 year old trichloroethene (TCE) dense non-aqueous phase liquid (DNAPL) source zone located within a heterogeneous sand/gravel aquifer at a UK industrial site is presented. The source zone was partially enclosed by a 3-sided cell that allowed detailed longitudinal/fence transect monitoring along/across a controlled streamtube of flow induced by an extraction well positioned at the cell closed end. Integrated analysis of high-resolution DNAPL saturation (S_n) (from cores), dissolved-phase plume concentration (from multilevel samplers), tracer test and permeability datasets was undertaken. DNAPL architecture was determined from soil concentration data using partitioning calculations. DNAPL threshold soil concentrations and low S_n values calculated were sensitive to sorption assumptions. An outcome of this was the uncertainty in demarcation of secondary source zone diffused and sorbed mass that is distinct from trace amounts of low S_n DNAPL mass. The majority of source mass occurred within discrete lenses or pools of DNAPL associated with low permeability geological units. High residual saturation ($S_n > 10\text{--}20\%$) and pools ($S_n > 20\%$) together accounted for almost 40% of the DNAPL mass, but only 3% of the sampled source volume. High-saturation DNAPL lenses/pools were supported by lower permeability layers, but with DNAPL still primarily present within slightly more permeable overlying units. These lenses/pools exhibited approximately linearly declining S_n profiles with increasing elevation ascribed to preferential dissolution of the uppermost DNAPL. Bi-component partitioning calculations on soil samples confirmed that the dechlorination product cDCE (cis-dichloroethene) was accumulating in the TCE DNAPL. Estimated cDCE mole fractions in the DNAPL increased towards the DNAPL interface with the uppermost mole fraction of 0.04 comparable to literature laboratory data. DNAPL dissolution yielded heterogeneous dissolved-phase plumes of TCE and its dechlorination products that exhibited orders of magnitude local concentration variation. TCE solubility concentrations were relatively localised, but coincident with high saturation DNAPL lens source areas. Biotic dechlorination in the source zone area, however, caused cDCE to be the dominant dissolved-phase plume. The conservative tracer test usefully confirmed the continuity of a permeable gravel unit at depth through the source zone. Although this unit offered significant opportunity for DNAPL bypassing and decreased timeframes for dechlorination, it still transmitted a significant proportion of the contaminant flux. This was attributed to dissolution of DNAPL–mudstone aquitard associated sources at the base of the continuous gravel as well as contaminated groundwater from surrounding less permeable sand and gravel horizons draining into this permeable conduit. The cell extraction well provided an

* Corresponding author at: School of Geography, Earth & Environmental Sciences, University of Birmingham, Birmingham B15 2TT, UK. Tel.: +44 121 414 3957. E-mail address: M.O.Rivett@bham.ac.uk (M.O. Rivett).

integrated metric of source zone dissolution yielding a mean concentration of around 45% TCE solubility (taking into account dechlorination) that was equivalent to a DNAPL mass removal rate of 0.4 tonnes per annum over a 16 m² cell cross sectional area of flow. This is a significant flux considering the source age and observed occurrence of much of the source mass within discrete lenses/pools. We advocate the need for further detailed field-scale studies on old DNAPL source zones that better resolve persistent pool/lens features and are of prolonged duration to assess the ageing of source zones. Such studies would further underpin the application of more surgical remediation technologies.

© 2014 The Authors. Published by Elsevier B.V. This is an open access article under the CC BY license (<http://creativecommons.org/licenses/by/3.0/>).

1. Introduction

Industrial use of trichloroethene (TCE) dates back to the early 1930s, some half a century prior to its recognition as a groundwater contaminant of major concern (Pankow et al., 1996; Rivett et al., 2006). Chlorinated solvents such as TCE may penetrate as a dense non-aqueous phase liquid (DNAPL) far below the water table to subsequently dissolve over decadal timeframes. They hence pose long-term threats to groundwater quality (Rivett et al., 2012; Rowe et al., 2007). The oldest TCE source zones may now be over 80 years old with potentially the majority over 40 years based on peak TCE production around the 1970s (Rivett et al., 1990) and poorest handling and disposal practices occurring prior to that time (Lyne and McLachlan, 1949; Pankow et al., 1996). Improved solvent management practices from the 1980s onwards, alongside declining TCE use, suggests that many TCE releases largely abated around 20 years ago if not earlier. Current investigation and remediation at sites may hence be targeting decades-old DNAPL source zones that have already undergone significant dissolution by natural groundwater flow (Parker et al., 2003). It is important to discern the field-scale nature of such old source zones to underpin predictions of their continuing longevity and remedial decision making.

Many laboratory and modelling studies (Chen and Jawitz, 2009; Christ et al., 2010; Glover et al., 2007; Grant and Gerhard, 2007; Oostrom et al., 2006; Parker and Park, 2004; Zhang et al., 2008) in addition to some controlled DNAPL-release field studies (Brooks et al., 2002; Hartog et al., 2010; Rivett and Feenstra, 2005), have shown persistent DNAPL is most likely associated with DNAPL pools or contamination in less permeable geological units from which mass transfer may be diffusion controlled. Pool-dominated rather than ganglia-rich source zones are expected to emerge with time as ganglia of distributed DNAPL more easily dissolve. Up-scaled mass transfer models initially developed for ganglia-dominated source zones, have been extended via a two-domain (ganglia and pools) source zone approach to account for the prolonged dissolution of high-saturation, pool-dominated source zone areas (Christ et al., 2010). With yet further time and eventual DNAPL depletion, reverse diffusion of contamination diffused into lower permeability zones may potentially lead to sustained concentrations above drinking water standards lasting decades (Seyedabbasi et al., 2012).

Detailed studies of actual DNAPL spill sites offer the potential to examine length and time scales beyond laboratory reach and validate models seeking to represent the field scale (Parker and Park, 2004). Detailed characterisation of DNAPL source zones increasingly exist courtesy of site investigation technology

advances (Mercer et al., 2010). These include direct-push (McAndrews et al., 2003), partitioning interwell tracer tests (PITTs) (Jackson and Jin, 2005; Johnston et al., 2013; Meinardus et al., 2002; Wang et al., 2013a, 2013b), high resolution coring and sampling (Meinardus et al., 2002; Puigserver et al., 2012), down-gradient plume monitoring via detailed monitored transects (Guilbeault et al., 2005) or extraction wells (Brusseau et al., 2007; Johnston et al., 2013). There remains, however, a lack of high spatial resolution datasets for actual spill sites that relate DNAPL saturation to accompanying dissolved-phase plume formation within the DNAPL source zone itself. Factors that control the detailed architecture, persistence and dissolution of old DNAPL source zones are important as they may influence assessment of the need for more surgical remediation technologies, selection of appropriate remediation performance metrics (concentration, mass flux or mass removal), assessment of the benefits of partial source zone removal as well as predictions of source strength with age (Blum and Annable, 2008; Chen and Jawitz, 2009; Parker and Park, 2004; Rao and Jawitz, 2003; Stroo et al., 2003; US EPA, 2003).

Our goal was to provide very detailed field-scale observation and discernment of processes controlling the architecture, persistence and dissolution of a 20 to 45 year old TCE DNAPL source zone at an industrial spill site. This was achieved by a novel field approach whereby the source zone was partially enclosed by a 3-sided sheet-pile cell that allowed detailed monitoring of 2-D longitudinal and fence transects along and across a controlled streamtube of flow through the DNAPL source zone. This allowed the removal of lateral flow transients that may cause significant concentration variability near source zones and confound interpretation of other processes (Davis et al., 1999; Rivett and Feenstra, 2005; Farrell et al., 1994).

2. Study site setting and methods

2.1. Research context and study site setting

The research presented is largely drawn from *Project Streamtube* (Rivett et al., 2010) that was undertaken under the umbrella of the larger research *Project SABRE* (Source Area BioREmediation) (Buss et al., 2010). *SABRE*'s main aim was to investigate field-scale bioremediation of a TCE DNAPL source zone (Zeeb and Houlden, 2010) in conjunction with supporting laboratory column (for example, Harkness and Fisher (2013)) and numerical modelling investigations (for example, Brovelli et al. (2012)). The so-called *SABRE Site* is located within a former chemical manufacturing plant in the UK (Fig. 1b). The studied source zone arose from a manufacturing plant that

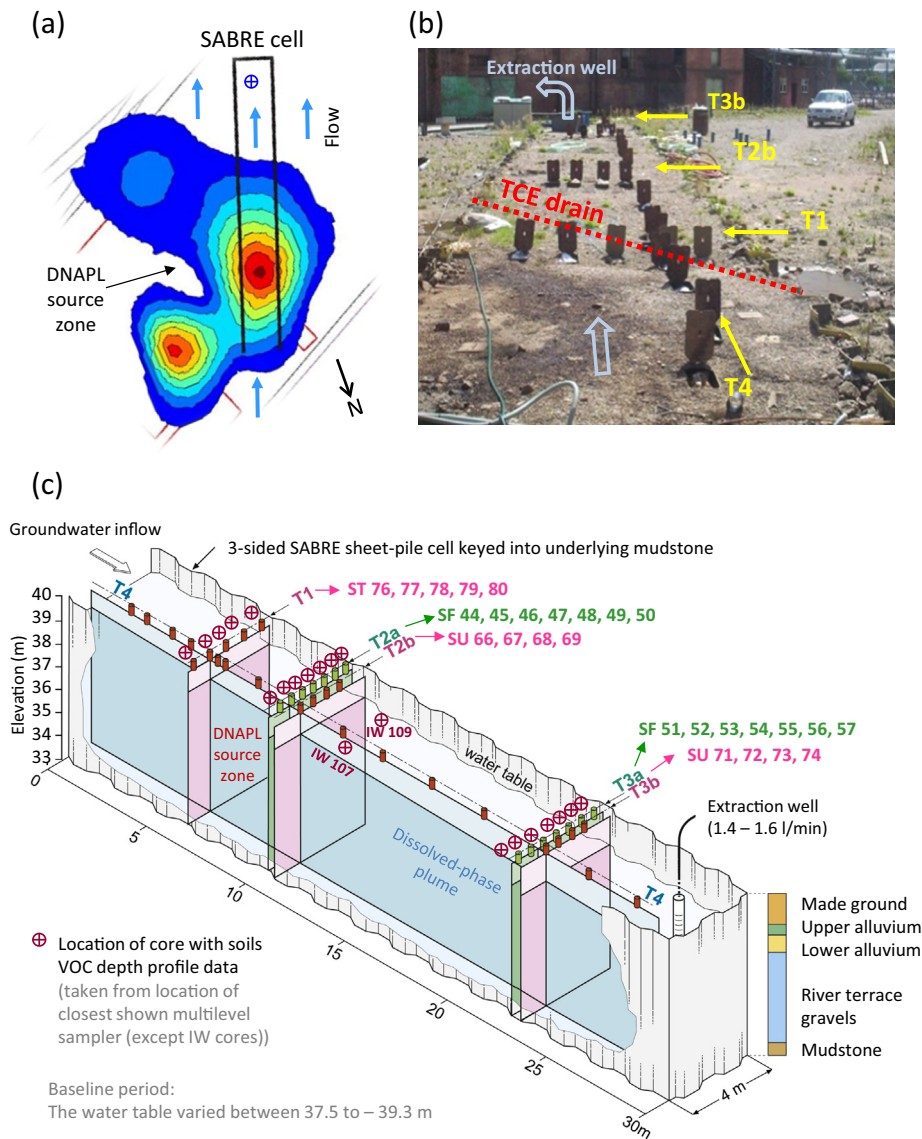


Fig. 1. Test cell showing: (a) location relative to source areas and area of DNAPL contamination delineated by prior site investigations (modified from Dearden et al., 2010a); (b) test cell looking down-gradient towards the extraction well; (c) instrumentation within cell pertinent to manuscript (modified from Rivett et al., 2010)—multilevel sampler transects are denoted by T with ST, SF, SU prefix numbered individual multilevel samplers in each cross-cell transect listed.

used TCE in the production process over its 1962–87 operational period. TCE releases from site effluent drains (Fig. 1b) and sumps were suspected over this period that was 20 to 45 years prior to our 2007–09 study.

The study site comprised towards 6 m of Quaternary upper/lower alluvium and river terrace gravels (RTG) superficial deposits with the lower 3–4 m being the main unconfined aquifer unit studied (Chambers et al., 2010; Lelliott et al., 2008) (Fig. 1c). Upper and lower alluviums were each around 1 m thick comprising silty clay and clayey silty sand respectively. The lower alluvium is lithologically similar to sandy zones within the underlying RTG into which it could gradationally change. The alluvium units are indicated by Chambers et al. (2010) to be variable in occurrence but generally encountered between 35.5 m to 38.5 m elevations and is overlain by gravels or made

ground and underlain by the RTG. The RTG of c. 2.7 m thickness was heterogeneous and poorly sorted with varied clay, silt and sand contents and contrasting layers of clean gravel and fine-grained low permeability horizons. The marked heterogeneity is attributed to an oxbow lake deposition environment of varying energy in close proximity. The d_{50} grain-size of the more gravelly layers was typically around 10 mm. Although some 'clean' well-sorted gravels were observed, grain-size distributions of frequently occurring poorly sorted samples typically spanned a 0.5 to 50 mm range. The unconfined aquifer is underlain by a very thick Mercia mudstone aquitard that exhibited moderate topographic variation of its upper surface.

The location of the sheet pile cell was guided by prior site investigations that had delineated an area of DNAPL contamination. Qualitative data on the vertical distribution of

contamination and depths of geological interfaces were obtained via combined membrane interface probe (MIP)–photoionisation detection (PID) and electrical conductivity profiling (Dearden et al., 2010a). The DNAPL source zone footprint delineated in the unconfined aquifer is indicated in Fig. 1a. Dissolved-phase TCE and biodegradation product cis-dichloroethene (cDCE), vinyl chloride (VC) and ethene (Ee) plumes extended from the source towards a river about 500 m away. Other contaminants released across the wider site included acetate that may have served as an electron donor for in-situ biodegradation.

2.2. Cell and research phases

Project SABRE installed a 3-sided “U” shaped polymer sheet-pile cell in the superficial aquifer deposits that was keyed into the mudstone to partially enclose the delineated TCE DNAPL source zone (Fig. 1b,c). The 30 m long by 4 m wide by c. 6 m deep cell was positioned to intersect the DNAPL source zone and aligned sub-parallel to the south–south west prevailing groundwater flow direction. The cell was open to groundwater inflow from the superficial aquifer at the up-gradient end with a forced gradient streamtube of flow established along the cell length by extraction wells installed at its closed end. The main suspected TCE leakage point cut across the cell at 3 to 7 m longitudinal distance (Fig. 1b) and hence the DNAPL source area was anticipated to be in the up-gradient-to-mid cell section allowing monitoring of its emitted dissolved-phase plume in the mid-to-down-gradient section. Although the total mass of TCE released (and dissolved over decades) was unknown, it was estimated from soil cores from within and local to the cell (including the data presented herein) that a median of 0.9 (10th–90th percentiles of 0.3–3.1) tonnes (t) of TCE was enclosed by the cell (Wealthall et al., 2010).

The cell was primarily set up to assess source area bioremediation (Zeeb and Houlden, 2010). Data reported herein were obtained prior to the bioremediation phase. Core–soil sampling was undertaken at various monitoring installations to establish the current (2007) source zone architecture during cell instrumentation. Groundwater sampling was undertaken to monitor current DNAPL source zone dissolution under pumped cell conditions during the baseline phase immediately prior to bioremediation implementation (Fig. 1c). The baseline phase extended from –97 d to 0 d (2 May 2007) when bioremediation commenced at day zero. The cell was pumped at 1.4–1.6 l min⁻¹ (2 m³ d⁻¹) during the baseline when the water table was typically 1 to 2 m below ground surface. For an approximate cell pore volume (PV) of 90 m³, a cell residence time of 42 d and a mean groundwater velocity of 0.7 m d⁻¹ is calculated. This velocity is comparable to estimates of the natural groundwater velocity across the wider industrial site. Around 2 cell PVs were removed during the baseline phase.

2.3. Groundwater monitoring

High resolution groundwater monitoring was conducted adopting multilevel sampler (MLS) approaches used in, for example, controlled release tests at the Borden site (Hartog et al., 2010; Rivett et al., 2001). MLSs were installed using a Sonicbore® percussion drilling (and coring) rig via a drive-tube lost-point method with surrounding formation re-collapse on

withdrawal. The dissolved-phase plume data reported herein were obtained during the baseline phase at –70 d, –49 d and –20 d prior to bioremediation onset from the T4 longitudinal transect of MLSs oriented along the cell axis offset from the centreline with cross-cell plume variability accessed via MLS fence transects T1, T2a,b and T3a,b (Fig. 1b,c). MLSs in T1, T2b, T3b and T4 comprised a central piezometer surrounded by 14 to 19 narrow (3.2 mm out. diam., 1.6 mm int. diam.) Teflon® tubes spaced at 0.3 m vertical increments. MLSs in T2a and T3a comprised 10 mm int. diam. tubes at 0.5 m vertical increments. The T4 transect contained over 200 sample points allowing a detailed 2-D slice of dissolved-phase plume concentrations through the DNAPL source area to be obtained. Constrained flow by the parallel cell walls meant that the groundwater monitoring should not be subject to concentration variability induced by wider site lateral groundwater flow direction variability. The majority of data reported herein were obtained from simultaneous sampling of ports on a given MLS via a low-flow suction manifold with 100–300 ml of water (depending on analysis needs) withdrawn allowing point aquifer sampling (White et al., 2008). Teflon®-septa capped vials were collected for chlorinated ethenes analysis via standard headspace GC–MS techniques.

2.4. Soils monitoring

The DNAPL source zone architecture prior to the baseline period was determined via 21 (Sonicbore®) cores (104 mm dia.) from within the cell. Core data were collected from transects T1, T2a, T3a and bioremediation injection wells (IW107 and IW109) located 13 m along the cell (Fig. 1b,c). Retrieved core lengths (150 cm) were sub-sampled at 5–10 cm increments with the exception of T2a and T3a cores that were subsampled at 50 cm increments. Micro-cored (1.4 cm dia.) sub-samples of 3 cm³ nominal volume were held in pre-weighed methanol-filled (Streamtube labs) or water-filled (SABRE labs) glass Teflon®-septa capped vials for VOC soils analysis via head-space GC–MS or GC–FID of (wet) total soils concentration analysis (White et al., 2008). DNAPL saturations were then estimated from total soil concentrations by partitioning theory (Feenstra et al., 1991) with percent DNAPL saturation of pore space (S_n) based on total TCE soil concentration less the maximum mass partitioned to aqueous and sorbed phases (later Table 1). It is recognised that investigation within any DNAPL source zone may compromise its original distribution, notably via DNAPL mobilisation deeper. We qualify the results where this was suspected as a potential influence. The thick mudstone was expected to provide an effective base. Only shallow DNAPL penetration into this unit was observed by Dearden et al. (2013) in their evaluation of the mudstone as a secondary source zone to the aquifer.

2.5. Supporting field tests

A conservative tracer test (Dearden et al., 2010b) was conducted involving potassium bromide tracer pulse injection into three wells positioned across the cell that were located 5 m down the cell (just up-gradient from transect T1). Each well was dosed with a total of 150 g of bromide over an 8-hour period with the calculated bromide input concentration after

mixing being $c. 600 \text{ mg l}^{-1}$. Temporal breakthrough curve monitoring was conducted 5.75 m from injection at MLS points in the down gradient transect T2a (Dearden et al., 2010b). A T4 longitudinal transect snapshot was also obtained at 6 d. Other field data drawn upon include falling-head slug tests on T2a and T3a transect MLS points of 10 cm screen section to determine hydraulic conductivity (K) via Hvorslev analysis (Cai et al., 2012; Chambers et al., 2010).

3. Results and discussion

3.1. Permeability field

Within the T2 transect source area, K varied over $<1\text{--}30 \text{ m d}^{-1}$ generally decreasing with depth to minimum values at 35 m elevation on the T4 cell side and 36 m on the opposing cell-side (Fig. 2a). A discrete high K gravel zone occurred at depth ($c. 33.7\text{--}34.7 \text{ m}$) within the RTG overlying the mudstone on the opposing cell side to T4. A shallow permeable horizon also occurred at 37–38 m and was expected to be an active flow regime during the baseline. Elevation-specific cross-cell heterogeneity was more pronounced at T2a (Fig. 2a) than T3a down gradient where cross-cell depth K profiles were more isotropic (Fig. 2b). A low permeability layer around 35.5 m elevation and the permeable gravel unit above the mudstone remained evident in T3a. Although the gravel was less conductive at T3a, it spanned the cell width with maximum values (15 m d^{-1}) now on the T4 cell side (Chambers et al., 2010). The deep gravel's potential as a preferential conduit is signified by its outlier position in Fig. 2c. Elevation-specific K maxima in T3a were around 50% of the T2a maxima at corresponding elevations and may have caused steeper hydraulic gradients at T3a (also induced by extraction well proximity) to maintain comparable water fluxes through each transect plane commensurate with extraction well discharge.

3.2. Conservative tracer test

The bromide tracer test confirmed the continuity of the permeable gravels overlying the mudstone via both rapid breakthrough over the 5 to 11 m cell interval monitored at T2a

(Fig. 3) as well as extensive bromide migration along T4 by 6 d. Early high-concentration breakthrough at T2a was primarily observed on the opposing cell side to T4 within the high K gravels at depth with a calculated velocity of $3\text{--}6 \text{ m d}^{-1}$ (or greater). Breakthrough was decreased, or absent, in MLS points within the less permeable units. Later breakthrough was characterised by broader, likely overlapping, breakthrough peaks ascribed to tracer advection and dispersion along different pathways. Combined breakthrough data for all MLS points exhibited a secondary broad peak arrival at $c. 10 \text{ d}$ corresponding to a velocity of 0.5 m d^{-1} with significant tailing. Breakthrough on the T4 cell side was less well defined and at reduced concentrations. Much tracer (and hence groundwater) bypassed the T4 cell side in the vicinity of the DNAPL source zone with preferred high-velocity passage through the more permeable units on the opposing cell side.

Observations of the longitudinal bromide plume migration after 6 d in T4 (Dearden et al., 2010b) revealed a mean velocity of 2.1 m d^{-1} (based on the tracer mass centroid) with rear portions of the plume moving at rates comparable to the cell extraction rate mean velocity of 0.7 m d^{-1} and faster portions maintaining velocities of $3\text{--}4 \text{ m/d}$ across the 5 to 25 m cell interval that were comparable to the high-velocity T2a breakthrough. Observance of tracer at 25 m along T4 at 6 d provided compelling evidence of hydraulic continuity of the deep gravel layer along the cell from the T1 injection area through T2 and to T3 including cross cutting the cell into T4 by that transect. Continued hydraulic connection of these gravels to the extraction wells was inferred and suggested a preferential conduit occurred through most, if not all, of the cell. The observed cross-cutting flow into T4, however, meant that the T4 transect could not be regarded in its entirety as a discrete streamtube (plane) of longitudinal flow.

3.3. DNAPL occurrence

DNAPL occurrence was primarily determined from soils total concentration data using partitioning-based estimates of TCE soil concentrations at which DNAPL may be present allowing for mass partitioning to saturated aqueous and sorbed phases (Feenstra et al., 1991). Calculated DNAPL threshold

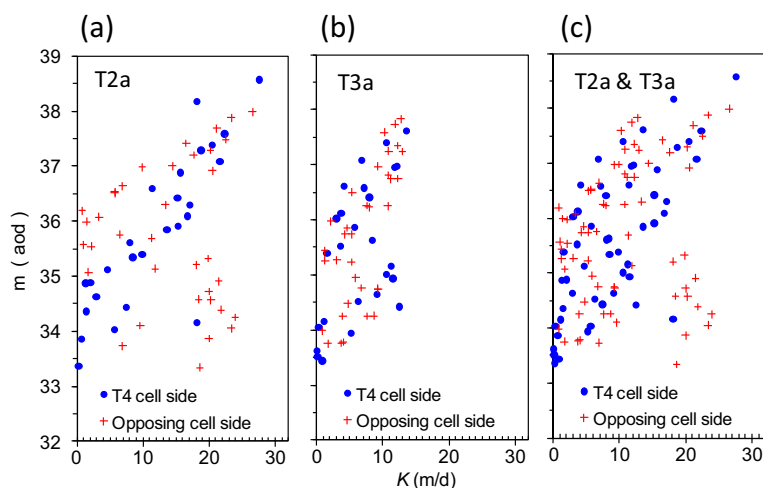


Fig. 2. Hydraulic conductivity variation with depth comparing T4 and opposing cell side data at transects: (a) T2a, (b) T3a, (c) T2a and T3a.

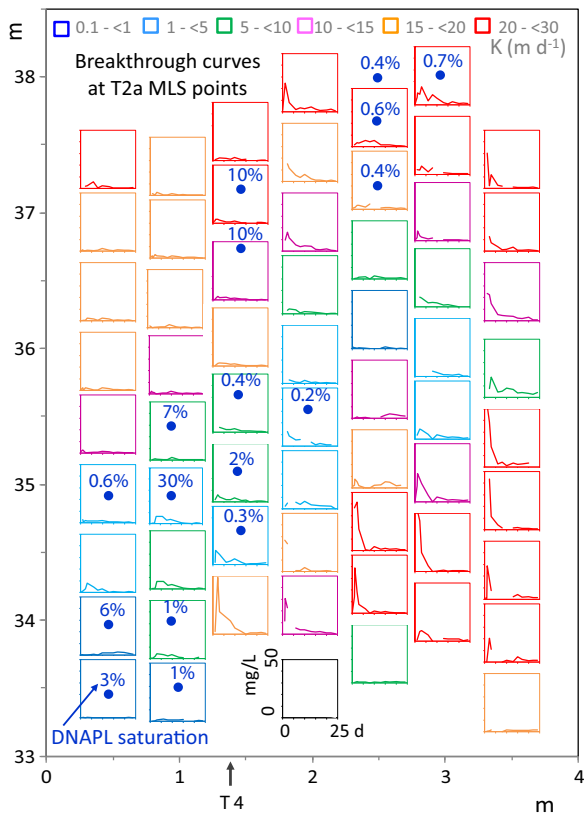


Fig. 3. Conservative bromide tracer test data showing Transect T2a MLS point breakthrough data (with colour-coded MLS point K values shown).

concentrations were sensitive to the sorption assumptions made. Table 1 uses a 98 sample f_{oc} dataset from T2a and T3a transects to calculate a selection of K_d sorption coefficients and a range of threshold values. In recognition of the threshold sensitivity to sorption and lack of f_{oc} data specific to each TCE soil concentration sample, subsequent analysis herein compares soil concentration field data to not only the arithmetic mean (AM) threshold of 606 mg/kg (for the 98 sample f_{oc} dataset), but also thresholds calculated at one and two standard deviations (σ) higher. Hence subsequent plots show three reference lines corresponding to the AM, AM + 1 σ , and AM + 2 σ threshold soil concentration values. Similarly, a trio of equivalent reference lines are calculated for DNAPL S_n values of 1% and 10% (10% lines coalesce on the log scale).

Confirmation that the calculated thresholds are reasonable indicators of DNAPL presence was provided by their good agreement with independent Sudan IV dye test data (Fig. 4). Other data from the SABRE site also endorse the utility of the Sudan test (Dearden et al., 2010a, 2013). Most, although not all, of the medium to high soil concentrations in Fig. 4 exhibit positive Sudan IV tests confirming DNAPL presence. The test also reliably indicated DNAPL absence for soil concentrations below the AM threshold. The AM + 1 σ threshold line at 1027 mg/kg approximately corresponds to the division between the ‘DNAPL absent’ and ‘DNAPL suspected’ Sudan IV results. Many of the suspected category points appear close to that line and hence, recognising that very low DNAPL

Table 1

Calculated wet-soil TCE concentrations for DNAPL threshold detection and 1% DNAPL saturation (1% pore-space saturation plus threshold partitioned mass) for various f_{oc} scenarios and assuming a porosity of 0.28, a particle soil density of 2.65 g/ml and TCE K_{oc} of 94 L/kg (US EPA (1996) incorporated within (US EPA, 2002). The estimates are developed from a 98 samples f_{oc} dataset from transects T2a and T3a.

f_{oc} used in calculation	f_{oc}	DNAPL threshold	1% S_n of DNAPL
(n = 98 samples in f_{oc} dataset)	%	mg/kg (wet)	mg/kg (wet)
Minimum	0.046	179	2007
Harmonic mean	0.26	374	2202
Geometric mean	0.37	471	2299
Arithmetic Mean (AM)	0.52	606	2434
AM + 1 σ (Standard deviation)	0.98	1027	2855
AM + 2 σ	1.45	1449	3277
Maximum	2.30	2220	4048

saturation may be difficult to practically observe in the dye test, a DNAPL threshold within the 606–1027 mg/kg (AM to AM + 1 σ) range is taken to be a reasonable demarcation of DNAPL presence.

Summary data on the frequency of occurrence and mass distribution of the 451 soil sample dataset obtained from core sections predominantly within the DNAPL source zone are shown in Fig. 5. Data are classified into ‘No DNAPL’, ‘Trace DNAPL (?)’, ‘Moderate residual DNAPL’, ‘High residual DNAPL’ and ‘Pooled DNAPL (?)’. The S_n values that delimit these categories are shown in Fig. 5. The ‘?’ reflects the fact that trace DNAPL may or may not exist in reality. Likewise in the highest category, the DNAPL may or may not be pooled. The three initial bars within each category are partitioned calculated using the AM, AM + 1 σ ,

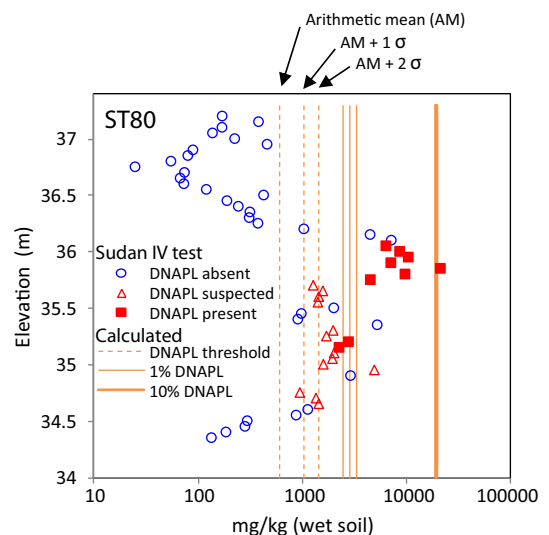


Fig. 4. Sudan IV test detection of DNAPL in core ST80 (Transect T1) shown relative to soil partitioning calculated DNAPL thresholds and 1% and 10% DNAPL S_n estimates. Lines for the arithmetic mean (AM) and AM plus 1 and 2 standard deviations (σ) are shown for DNAPL threshold, and 1% and 10% S_n (with the 3 lines mutually eclipsed in the 10% S_n case). Variations for each reflect the influence of the site-measured variation in f_{oc} (Table 1).

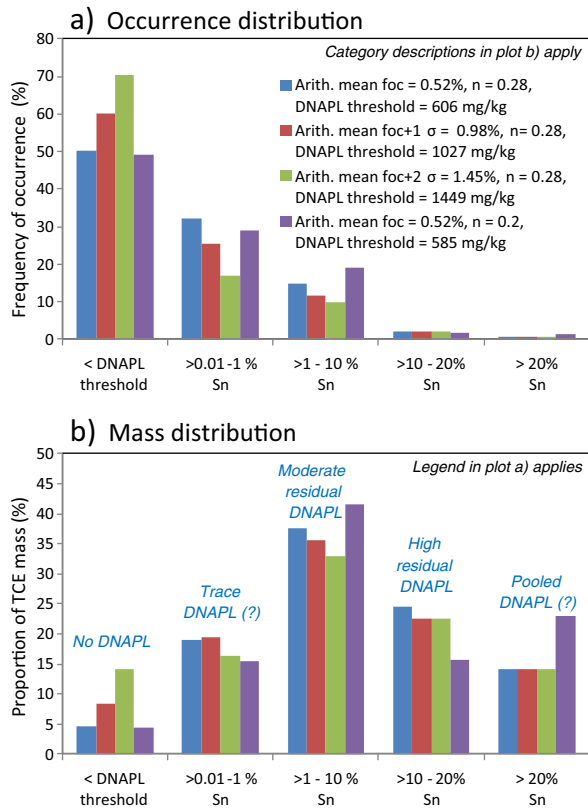


Fig. 5. Distribution across S_n categories of TCE soil concentrations observed in all pre-baseline core (451 soil samples) showing: a) sample occurrence; and b) TCE mass distribution. Distributions are shown for varying assumptions on f_{oc} (Table 1) that influence the category boundaries and hence mass and number allocated.

AM + $2\sigma f_{oc}$ -based approach described above, the fourth bar uses the AM f_{oc} but with a reduced porosity. Fig. 5a illustrates that around 50–70% (different bars) of the source area sampled did not contain DNAPL and that a further 20–30% only contained trace DNAPL up to a saturation of 1%. The relative balance between these categories is sensitive to the threshold value used. The source area is hence dominated by DNAPL-free zones and areas where DNAPL is only present at trace quantities, or alternatively absent if sorption values are greater than expected.

The source area is old and certainly diffused mass into say the intraparticle porosity of the solid-organic matter could be high and sorption greater than suggested by our f_{oc} - K_{oc} estimate (higher K_{oc} values exist in the literature—we use a geometric mean of 94 L/kg compared to an average of 57–150 L/kg ($n = 21$) (US EPA, 1996, 2002)). Nevertheless our approach of using a range of f_{oc} data and thresholds at AM + 1σ , AM + 2σ does accommodate, to some extent, the influences of higher sorption coefficients arising from other non-ideal influences such as non-linear sorption (Rivett and Allen-king, 2003; Wang et al., 2013a, 2013b) or else inferred from desorption experiments using long-term contaminated site samples (Riley et al., 2006). Although the dye test data (Fig. 4) do support some of the ‘Trace DNAPL’ samples contain DNAPL, saturations less than c. 1% do need to be treated with some caution in the absence of sample-specific K_d data.

The uncertainty in DNAPL thresholds and sorption coefficients also means that precise demarcation of the secondary source zone mass (diffused mass to lower permeability, DNAPL-free, geological units) and the exact allocation of masses between mass phases or compartments (for example, in useful approaches such as the ‘14 component model’ for site assessment (Sale and Newell, 2011)) may be challenging. This uncertainty is reflected in the varying assignment between ‘No DNAPL’ and ‘Trace DNAPL (?)’ categories in Fig. 5. The need for methods that reliably determine the presence of low DNAPL saturations and or sorption parameters specific to soil samples is endorsed if the goal is the precise segregation of secondary source zone and DNAPL source zone masses. Alternatively, and more practically viable perhaps, definition of the secondary source zone could be expanded to include the presence of trace DNAPL. Whilst not ideal in some respects, there is some justification for this in that the release from both secondary source sorbed mass and trace amounts of DNAPL (<1% S_n) may largely be diffusion controlled.

Saturation categories exceeding 1% S_n become increasingly insensitive to the sorption assumptions at greater saturations as illustrated by the initial three bars that show comparable moderate residual, high residual and pooled DNAPL values for each of these categories (Fig. 5a). The distribution of saturations over 1% does, however, exhibit some sensitivity to the porosity assumption as shown by the 0.2 porosity values (4th bar). The determination of increased saturation values and, for example, whether a DNAPL is likely at a saturation indicative of pooling (and hence mobility), will be sensitive to the porosity assumption. Within the present dataset and range of partitioning calculations used, the ‘Moderate residual DNAPL’ category accounts for 10–19% of sample occurrence. ‘High residual DNAPL’ and ‘Pooled DNAPL (?)’ categories together account for just 2.7–2.9% and illustrate the localised occurrence of high saturations within the source zone area (Fig. 5a).

The majority of TCE mass is accounted for by the categories with saturations over 1%. The predominant mass, 33–42%, is within the moderate residual DNAPL category (Fig. 5b). The high residual saturation category, although <3% of occurrence, accounted for nearly 25% of the mass. Pooled DNAPL, at c. 1% occurrence, accounted for 14% of the mass for a porosity of 0.28, but increased to 23% of the mass for the lower porosity of 0.2. Hence the source zone is characterised by most of the mass being in relatively localised portions of the source; saturations over 1% contain 70–80% of the source mass but are located in just 13–22% of the source sampled volume. The localised nature of this mass, particularly the high saturation or pooled DNAPL, may lead to significant potential to underestimate source zone mass where site investigation data are sparse or even at moderately high spatial density.

In relation to scoping secondary source zone mass importance, if this was approximated to equate to the ‘No DNAPL’ category, this amounts to 5–14% of TCE source mass and some 50–70% of the source volume (Fig. 5). Expanding the secondary source mass to additionally include the ‘Trace DNAPL (?)’ category would lead to it accounting for 24–31% of the source mass and some 78–88% of the source volume. In practice, however, the secondary source mass of most long-term concern will be associated with the discrete lower permeability horizons within this greater volume. The need to hence combine chemical

concentration data with high resolution geological log and permeability data is duly recognised in the assessment of the nature and persistence of the secondary source zone at the field scale and confirm its importance relative to laboratory and modelling studies that point to its long term impact over decades (Seyedabbasi et al., 2012). Study of the secondary source zone at this site has primarily focused upon contamination in the immediate underlying mudstone near the cell (Dearden et al., 2013) in preference to the complexity of discrete low permeability horizons within the cell aquifer unit itself (see Sections 3.4 and 3.5).

3.4. Architecture

The summary data in Fig. 5 and discussion above confirm that much of the source zone was characterised by areas of very low, even absent, saturations of DNAPL. These were existent alongside elevated saturations which, although rarely occurring, still accounted for the majority of DNAPL mass delineated. Total source zone mass estimates are hence very dependent upon investigations locating these discrete layer, high mass, zones. The uncertainty in our estimation of DNAPL present in the cell provided earlier (Section 2.2) is hence not unexpected. Indeed, if several discrete DNAPL layers were missed then the source mass actually present could conceivably be even greater than the mass range estimated. Controls on the detailed architecture of the delineated TCE mass and calculated saturations (based on Table 1) are discussed below.

3.4.1. Architecture–permeability control

The detailed TCE source zone architecture is indicated by soil core depth profiles from orthogonal transects T1 and T4 through the source zone (Fig. 6). T1, located 5 m along the cell at the former drain-sump source, indicated DNAPL with localised exception was not encountered at >36.5 and <33.5 m elevations (although not all cores reached the underlying

mudstone). Between these elevations, many concentrations were above the DNAPL detection threshold, but still at very low S_n (<1%). The majority of higher S_n (>1%) was restricted to the 34.5–36.5 m interval. Greatest saturations were found at 35–36 m with S_n > 20% tentatively assumed to be indicative of pooled DNAPL accumulations. The original spill was conceptualised as a drip leakage with DNAPL expected to have preferentially migrated along the more permeable pathways. Permeability control of observed architecture is demonstrated through comparison of cross-cell T2a K profiles with S_n profiles from T2a and nearby T1 (Fig. S1), recognising some uncertainty of K data extrapolation to T1 at 4 m away (all data are shown in Fig. S1 with some of these profiles compared with other data in later manuscript figures). S_n occurrences (>0.2% S_n) are also plotted in Fig. 3 that allows comparison of DNAPL location with both the permeability and tracer velocity fields.

Less permeable layers ($K < 2.5 \text{ m d}^{-1}$) prevalent in the T2a source area at 34.5–36 m are particularly influential of source zone architecture. S_n peak occurrences >3% invariably occurred within or immediately above these low permeability layers located at decreasing elevations towards the T4 cell side (Figs. 2, 3, S1b,f,g). Although the (laterally spaced) multiple core data in Fig. 6a give the impression of a 1.5 m thickness of DNAPL, the individual core data indicate DNAPL is present as discrete layers with the greatest continuous thickness of DNAPL at >1% saturation being 0.5 m observed in ST79 that has a maximum S_n of 23% (Fig. S1f). Rapidly decreasing S_n generally occurred with increasing penetration depth into the low K unit that might be reasonably ascribed to restricted DNAPL invasion during initial release where capillary pressures generated would have been modest in this shallow aquifer system. Within the overlying more permeable units, S_n likewise decreased, but at a more linear and modest rate. The apparent large thickness of DNAPL in Fig. 6a is attributed to the supporting low K horizons varying with elevation across the cell (Figs. 2, S1).

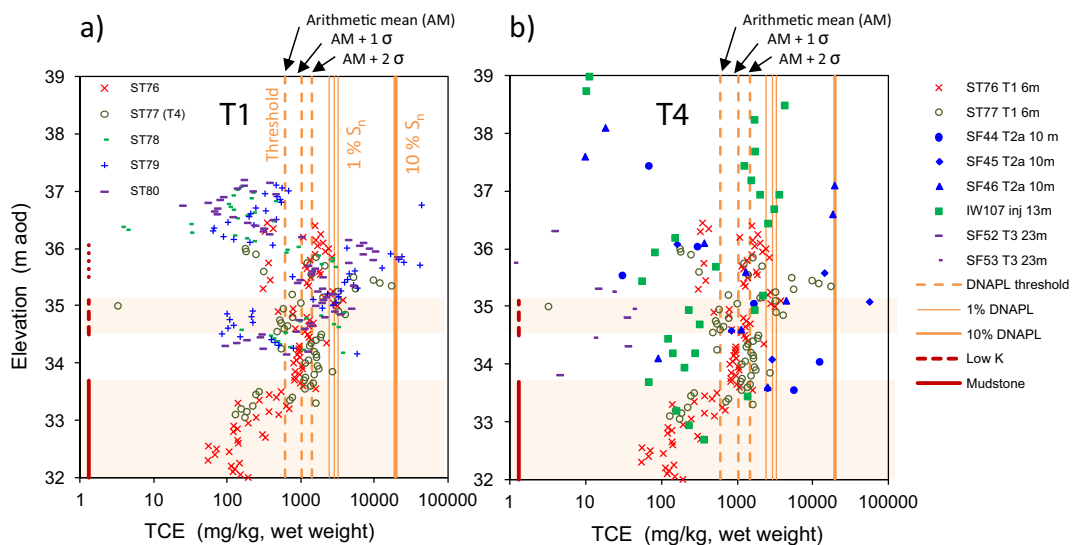


Fig. 6. TCE soils concentration profiles for Transects (a) T1 and (b) T4 core shown relative to low permeability geological units and estimated lines of DNAPL saturation (S_n) (see Fig. 4 caption). The low K (hydraulic conductivity) layer is marked at an indicative elevation as it varies locally (see later Fig. 13).

Comparison in Fig. 7 of core profiles containing elevated S_n occurrences (potentially pooled or previously pooled but now depleted DNAPL horizons) revealed that peak S_n layers occurred within strata that were permeable, based on the annotated log descriptions, relative to the immediate underlying (arresting) unit. For example, in SF45 the DNAPL is predominantly in sandy gravels that overlie a silty sand; in ST 77, it is within gravels overlying silty gravels; and, in ST80, within sand–fine to medium gravels overlying sand. These incidences (and respective K data in Fig. S1) suggest that strata

underlying the accumulated DNAPL do not necessarily need to be very low permeability, but rather of sufficient permeability contrast with the overlying more conductive unit to allow preferential lateral DNAPL spread in that layer and accumulation above the lower permeability interface during the original release event. The low permeability units have been variously penetrated and themselves may contain around 1–3% S_n with even lower saturations (to below DNAPL threshold) found in the deeper, typically more gravel-based units. Those low values reflect either an original

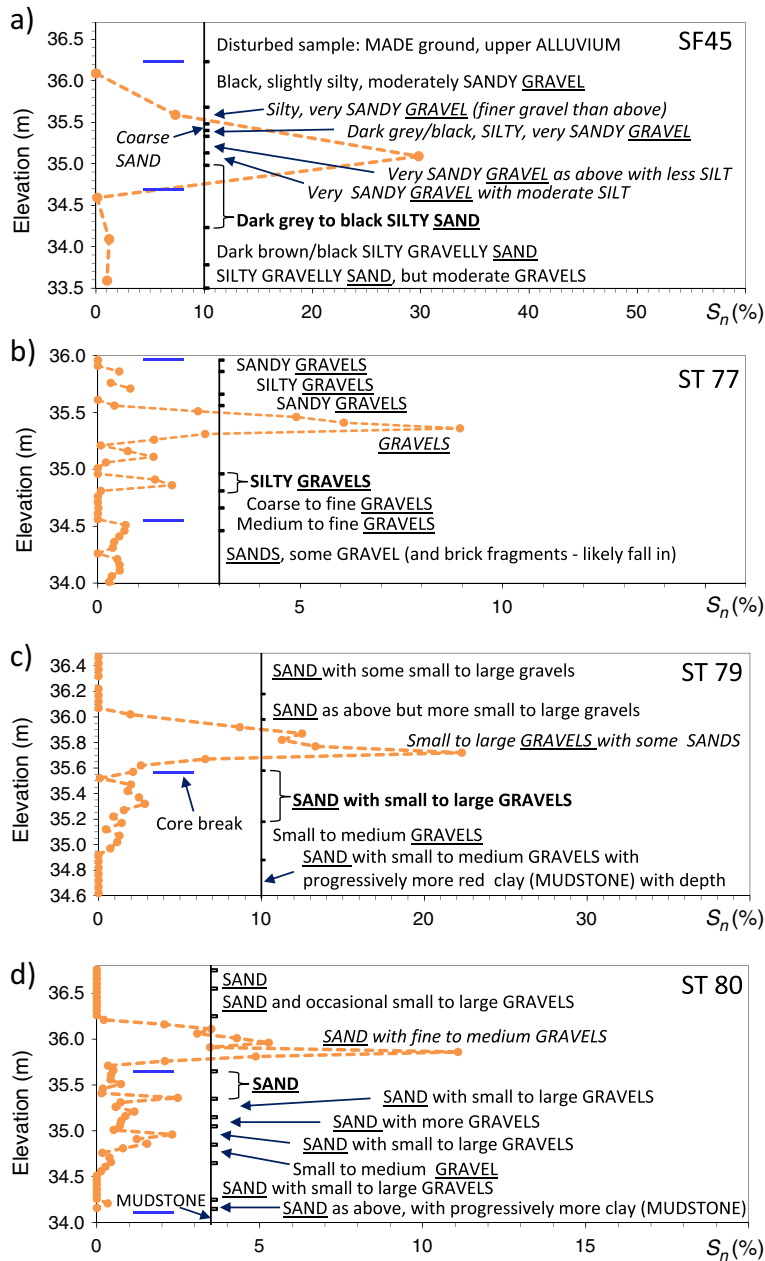


Fig. 7. Pre-baseline period DNAPL saturation (S_n) core profiles shown relative to geological log descriptions for transect T2a cores at: (a) SF45, and for transect T1 at (b) ST77, (c) ST79, (d) ST80.

absence of DNAPL and or facile historical dissolution of DNAPL previously present.

The predominant occurrence of persistent DNAPL within more permeable strata rather than within the immediate underlying lower permeability strata is an important observation. It suggests DNAPL is persisting in permeable strata due to: the reduction in strata permeability arising from DNAPL presence; facile bypassing of DNAPL via overlying more permeable strata; and/or, the underlying supporting lower permeability layer only allowing predominant diffusion-based release.

3.4.2. Architecture: mudstone interface control

Some cell core provided evidence of DNAPL at the mudstone interface (although not all core reached this interface at around 33–34 m elevation) with sharp, relatively log-linear, concentration declines into the mudstone aquitard indicating it to be a significant barrier to DNAPL penetration. A separate mudstone investigation close to the cell likewise confirmed DNAPL presence at this interface with lower concentrations indicative of dissolved/sorbed TCE decreasing into the mudstone (Dearden et al., 2013). Several cores (Figs. 6, S1 and Dearden et al., 2013) exhibited modest S_n increases at the interface although the 7% maximum was not indicative of pooling. Our review (Supplementary Material, Fig. S2) of available core and MIP data (Dearden et al., 2010a, 2013) suggests DNAPL could be relatively widespread at the mudstone interface. Profiles near the gully-drain sump line-source exhibited DNAPL both within the immediate overlying units and at the mudstone interface. These were surrounded by a perimeter of profiles exhibiting DNAPL evidence only (or predominantly) at the mudstone interface.

The above would accord with greater lateral DNAPL spread with penetration depth and greatest ultimate spreading associated with the continuous mudstone interface for a fully penetrating spill. Lower permeability layers at intermediate elevation in the cell (Figs. 2, S1) may prevent DNAPL penetration to the mudstone locally. However, the observed heterogeneity and oxbow lake deposition environment suggests that such layers are unlikely to be that laterally extensive and penetration to the shallow mudstone is generally probable. This will either have occurred via some lateral diversion on these layers and overspill or via more direct vertical pathways where intervening low permeability layers are absent. Perimeter spread on the mudstone appears to be around 10–15 m radially from the line source with the spread diameter of up to 20–30 m corresponding to 3–5 times the depth to mudstone (6 m). This spread ratio appears not unreasonable considering the long-term DNAPL slow (drip) release mode, layered aquifer heterogeneity, lateral continuity of intervening low K layers and varied mudstone topography (Chambers et al., 2010; Dearden et al., 2010a). It is speculated that high S_n values indicative of interface pooling could easily be missed due to their discrete spatial occurrence in mudstone topographic lows, or poor core (and or DNAPL) recovery sometimes potentially encountered at the gravel–mudstone interface.

3.4.3. Architecture: longitudinal transect observations

The architecture in the longitudinal (flow) direction in transect T4 (Fig. 6b) displayed similarity at T1 (6 m) and T2a (10 m) transect intersections suggesting continuity of TCE–

DNAPL lenses ascribed to lateral continuity of lithologies. The maximum S_n of 30%, found in SF45 at 10 m along T4 (Fig. 1c), was ascribed to DNAPL pooled within and over the minimum K layer at 34.5–35 m (Figs. 2b, S1b). This low K layer appears to sharply dip across the cell at T2a possibly levelling out at T4 (compare Fig. S1a–e; Chambers et al., 2010) and may have resulted in DNAPL laterally draining and pooling on this interface around T4. The most significant DNAPL accumulation detected along T4 in both T1 and T2a was associated with this 35–35.5 m elevation layer. Where S_n was >1%, saturations at specific elevations were consistently greater in T2a than T1 (Fig. 6b (note legend differentiates)) and is consistent with expected preferential DNAPL dissolution from more up-gradient parts of the source and, with time, the centre of mass of the depleting source migrating very gradually down gradient. The above and wider site investigation data (Fig. 1a) suggest DNAPL was largely within the 5–10 m T4 interval. By 13 m, the source appeared fairly limited with DNAPL only approaching 1% S_n at c. 36.5 m and 35 m elevations coincident with peak saturations up-gradient, again suggesting layered geological control of the architecture. The source extent directly up-gradient from T1 was not determined although Fig. S2 suggests some DNAPL presence laterally up gradient of the cell.

3.4.4. Mobile DNAPL and installation influence on architecture

DNAPL S_n exceeding c. 20% (an indicative literature residual S_n and threshold for pooling) were rarely detected (Fig. 5a), but may be mobile. During groundwater sampling events, DNAPL fluid was only observed in samples retrieved from MLS SF44; initially from just the deepest point, but subsequently from 33–35 m elevation points (lower left-side of Fig. 3; Fig. S1a). Although S_n values (<7%) did not infer mobile DNAPL presence, core recovery was poor at depth (0.5 m recovered of 2.4 m cored) but exhibited strong solvent odours. Also, SF44 was located 0.5 m from SF45 where a maximum S_n of 30% was detected at 35 m elevation (Fig. S1b). Plume concentrations over the subsequent 600 d baseline/bioremediation persisted as a rather odd looking vertical column of high concentrations around the deep SF44 points (Cai et al., 2012; Chambers et al., 2010). Low K values, possibly influenced by DNAPL presence and or lost mudstone during coring, were similarly distributed in the vertical (later Fig. 13). We speculate some DNAPL drainage occurred from the 35 m high S_n layer, into the annulus of SF44 with accumulation assisted by the local low permeability conditions (and nearby cell wall potentially).

Coring and MLS installations were not anticipated to have compromised observed DNAPL distributions at shallow to mid aquifer depths, but may have influenced deeper profiles, for example, below the c. 35 m elevation low K unit. Comparison of S_n profiles above and below core breaks in Fig. 7 provides some insight on possible DNAPL mobilisation to depth. Cores ST45, ST79, and ST80 (Fig. 7a,c,d respectively) exhibit low saturations in the deeper core with minima below the core break shown with some profile sections below DNAPL thresholds and trends that were generally consistent with geological expectations. Hence, they do not support significant DNAPL mobilisation occurred to depth. Core ST77 (Fig. 7b) does, however, show an obvious step S_n increase immediately below the core break. The

increase was limited to approaching just 1% S_n . Overall, it is difficult to prove influence, or not, of installation works on the observed DNAPL architecture. The above suggests influence may be slight. Some caution, nevertheless, in the interpretation of the deeper aquifer data is warranted.

3.5. DNAPL persistence: characterisation of high saturation lenses/pools

S_n data in T1 were vertically resolved at 0.05 m increments and provided opportunity to evaluate architecture of the high saturation DNAPL lenses (potentially pools) persisting decades after spillage in the more up gradient portion of the source zone (Fig. 8a). S_n profiles are shown for ST77, 79 and 80 that are up to 0.5 m thickness (for $S_n > 1\%$) associated with the aforementioned 35–36 m low K layering. Differing profile depths reflect the dipping of the low K layer across the cell (Figs. 3, S1). To allow data inter-comparison, profiles are shown normalised to their individual maximum saturation S_n^{max} values plotted with vertical distance from their S_n^{max} layer elevation (Fig. 8b). The normalised profiles collapse to comparable distributions revealing a fairly linear saturation decline above the S_n^{max} layer (dashed reference line) to near zero saturation values over about 0.25–0.4 m. These contrast with the deeper profiles in the geologic units below the S_n^{max} layer that show more rapid, more exponential, declines over about 0.2 m to low saturation values, but with some variable persistence up to c. 0.1 S_n/S_n^{max} normalised values when distances up to 0.4 m are examined. In each of the three cases, around 80% of the TCE mass is present at elevations above (and including) the S_n^{max} layer and 20% below this layer. Such observations are important in assessing long-term dissolution potential, surgical targeting of remediation technologies and the importance of secondary source zone mass.

Noting axes are reversed to Fig. 8b (to allow saturation to be expressed as a function of distance), linear best fits to the data above S_n^{max} layer are shown in Fig. 8c and exponential best fits to the data below S_n^{max} layer in Fig. 8d. The equations given provide a reasonable quantitative description of the DNAPL architecture evolved within the high S_n lenses underlain by a low K supporting unit. The similarity in linear gradient fit to ST79 and ST80 is attributed to their proximity. The gradient for the more laterally located, lower elevation ST77 profile is steeper presumably reflecting a different geological and or spill-evolution environment. The equations and goodness of fit depend on whether the lines have forced intercepts. S_n may be estimated as a function of d , the vertical (z) distance from the S_n^{max} layer, for ST77 by:

$$S_n/S_n^{max} = -4.10 d + 0.94 \quad (R^2 = 0.97)$$

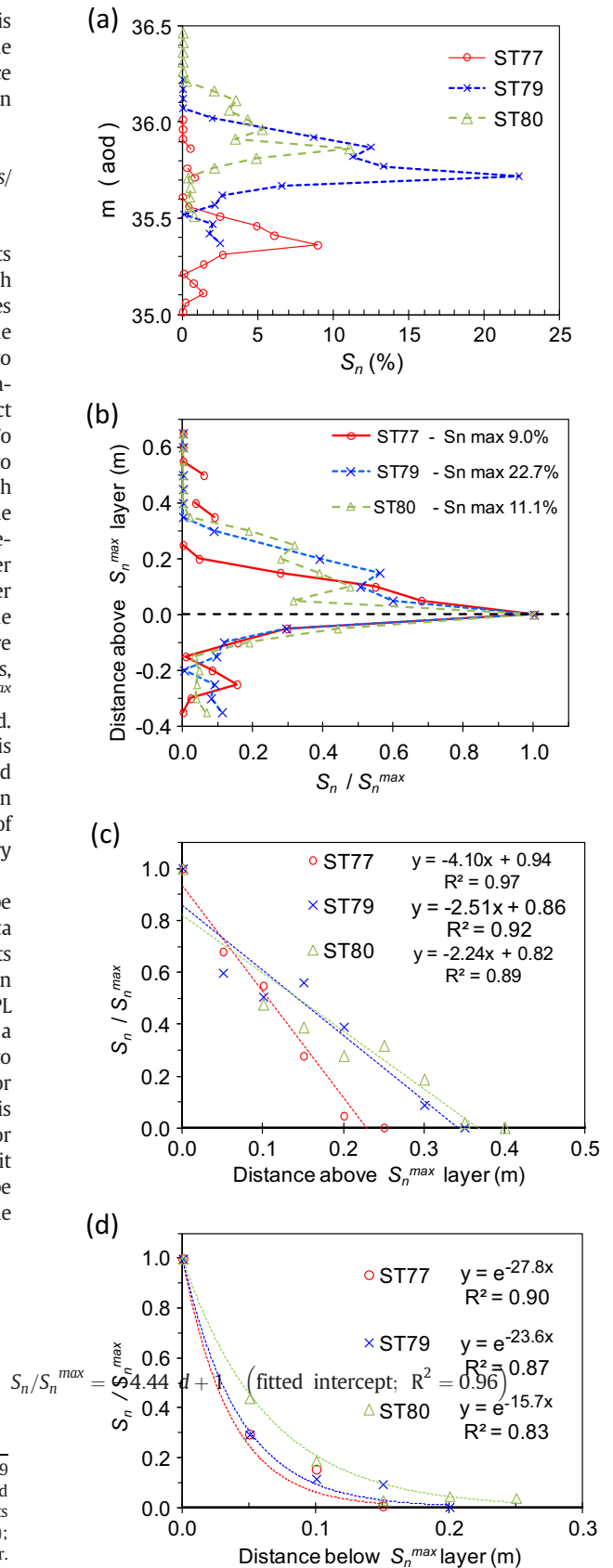


Fig. 8. Evaluation of elevated DNAPL saturation layers in T1 profiles ST77, ST79 and ST80: (a) S_n depth profile (part of); (b) S_n data normalised to S_n^{max} plotted with vertical distance (d) from the S_n^{max} layer locality; (c) linear best fits to plots of S_n^{max}/S_n versus distance d above S_n^{max} layer (one outlier removed from ST80); (d) exponential best fits to plots of S_n^{max}/S_n versus distance d below S_n^{max} layer. Note distance axis is switched for (c) and (d) relative to (b).

and, for ST79 and ST80 together by:

$$S_n/S_n^{max} = -2.35 d + 0.84 \quad (R^2 = 0.90)$$

$$S_n/S_n^{max} = -2.93 d + 1 \quad (\text{fitted intercept; } R^2 = 0.83)$$

The evolved S_n distribution will relate to a combination of factors, including: the initial DNAPL release mode; the geologic permeability field that influences initial accumulation within the higher K layers and any penetration into the underlying (supporting) low K units; the geological- and S_n -controlled permeability field that subsequently controls dissolution of the DNAPL; source age and degree of dissolution to date; and, location along a pooled accumulation. From the earlier observations of predominant DNAPL occurrence in the higher permeability units, it is reasonably assumed that the S_n^{max} layer occurs at the low permeability geological interface that acted as a capillary barrier to vertical DNAPL migration during historic release. Whilst comparison of the aged DNAPL profile to its initial spill condition cannot be made locally, it can still be compared to field-research site intentional releases of DNAPL. For example, our observed DNAPL profiles reasonably compare in shape to the spill by Hartog et al. (2010) at the Borden sand aquifer site. Their core data similarly exhibits layers of non-aged DNAPL that, somewhat irregularly slowly increase with depth to maximum saturations that then sharply decline.

The observed approximate exponential decline in S_n below the S_n^{max} layer presumably reflects some local variability of DNAPL entry and or diffusion-based entry into that layer. Due to the combination of these processes occurring, uncertainty in sorption coefficients and DNAPL thresholds (Section 3.3) and the moderate resolution of the thin lower K intermediate layers within the cell as well as coarser resolution of the aqueous phase (compared to these soils data), we provide a simple exponential fit rather than attempt a diffusion-based simulation of these soil concentration profiles. Concentration profiles within the underlying mudstone (Fig. 6, for example, shows DNAPL saturations underlain by aqueous/sorbed phase concentrations below the DNAPL threshold that appear diffusive) do, however, provide a clearer opportunity to evaluate DNAPL penetration, diffusion and back-diffusion. In this regard, we refer the reader to the mudstone study undertaken by Dearden et al. (2013) in the vicinity of the cell.

Observed DNAPL heights of 0.25–0.4 m above the S_n^{max} layer are commensurate with those expected from a former pooled DNAPL accumulation. Maximum heights of TCE DNAPL above a sub-water table capillary barrier (Kueper et al., 2003) were 0.4 m for a 1 m/d conductivity fine sand and 0.75 m for a 0.1 m/d silt. Although more high resolution and local K data would be required to fully resolve the flow environment through and over the (pooled) DNAPL accumulation, available data (Fig. S1) suggest greater intrinsic permeability of the sediments and permeability to the wetting fluid (water) with vertical distance above the S_n^{max} layer will have increasingly facilitated dissolution of the uppermost DNAPL most distant from the S_n^{max} layer. Increased permeability of the uppermost DNAPL layers with respect to the wetting phase, i.e., water flow, will occur with time as the DNAPL depletes and will further facilitate the dissolution of the remaining DNAPL.

3.6. DNAPL source zone: dechlorination product partitioning

Dechlorination products cDCE and VC, not expected in the TCE originally released, were observed in pre-baseline source area cores as exemplified by the ST79 core in Fig. 9. As well as being present in migrating groundwater sampled in the pore water and in the sorbed phase, cDCE and VC may reversibly partition to DNAPL present. Ramsburg et al. (2010) provide laboratory and supporting model evidence for the significance of this dynamic exchange for VC in TCE DNAPL and cDCE in PCE (tetrachloroethene). However, field-scale evidences of this phenomenon are lacking. Example ST79 total soils concentration data (Fig. 9a) illustrate VC is at very low concentrations alongside cDCE at moderate values up to 500 mg/kg and slightly higher (up to c. 3000 mg/kg) in other core collected. Only rarely do cDCE soil concentrations exceed TCE that is usually present at 1–2 orders of magnitude greater concentration.

Total soils concentration mole fraction (X) plots (Fig. 9b) indicate X_{TCE} is typically >0.95 and $X_{cDCE} <0.05$ (with X_{VC} negligible) (mole fraction here is not within a specific phase, but rather the molar proportion of each compound present in the bulk soil sample and hence, $X_{TCE} + X_{cDCE} + X_{VC} = 1$). Notably, X_{TCE} and X_{cDCE} profiles exhibit marked, mirror image, gradient changes at the DNAPL interfaces indicated in Fig. 9 that were based on the independent TCE DNAPL threshold analysis. These mole fraction data hence appear to provide important corroborating evidence of that interface. Fig. 9c focuses upon the mid-horizon DNAPL accumulation that notably exhibits a discrete increase in cDCE at 35.8 m that is around 2–300 mg/kg higher than the relatively uniform profile above and below this elevation. This is interpreted to be indicative of an accumulation of cDCE associated with the DNAPL in this vicinity (Fig. 9a). Fig. 9c plots X with distance above the S_n^{max} layer (per earlier Fig. 8) and demonstrates a very gradual, near linear, increase in X_{cDCE} from 0.01 at the S_n^{max} elevation to 0.06 at the upper surface of DNAPL. There is a corresponding X_{TCE} decrease over this 0.3 m vertical interval where there is a fairly linear depletion in S_n (discussed earlier). Immediately above the DNAPL, within the main aqueous-phase plume, X_{TCE} shows a much increased, still near linear, decline to zero over 0.25 m and a corresponding increase in X_{cDCE} (Fig. 9c). The latter subsequently declines at the highest elevation with a corresponding increase in X_{VC} . These data hence show strong evidence of dechlorination activity that predominantly occurs within decimetres immediately above, rather than within, the DNAPL. We expect groundwater flow to be lateral, rather than vertical, through this locality and we interpret the profile to be monitoring the dissolution, dispersion and dechlorination of the dissolved-phase plume emitted from similar elevation DNAPL located (a short distance) up gradient.

The X_{cDCE} and X_{TCE} profiles associated with the DNAPL at depth on the mudstone show extremely similar values, gradients and gradient inflections to the mid-horizon DNAPL profiles, including an eventual decline in X_{cDCE} and increase in X_{VC} (Fig. 9b, 34–34.7 m). The main difference is that the DNAPL S_n thickness does not full cover the low gradient X_{cDCE} and X_{TCE} profiles. It is quite possible, that DNAPL was not fully recovered at the base of this core which could explain this discrepancy. The above examples illustrate the potential utility of X_{cDCE} and X_{TCE} data to corroborate the DNAPL interface and exchange processes occurring.

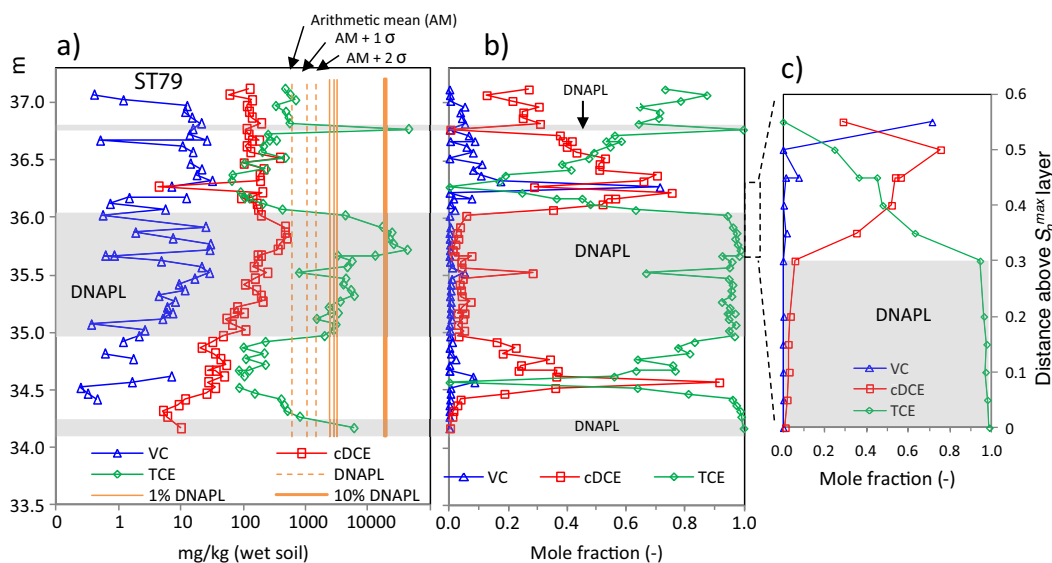


Fig. 9. Pre-baseline core ST79 (Transect 1) soil sample depth profile data for TCE, cDCE and VC showing: (a) soil concentrations relative to calculated DNAPL thresholds and 1% and 10% S_n estimates (see Fig. 4 caption); (b) total soil concentrations expressed as bulk mole fractions (proportions) (see text); and (c) Inset of mole fraction data plotted with distance above the S_n^{max} layer at 35.7 m elevation showing contrast in mole fraction gradients at the DNAPL interface (the grey-shaded area in all figures denotes DNAPL presence at TCE soil concentrations exceeding the AM + 1 σ threshold (Table 1)).

3.6.1. Predicted phase-partitioning of cDCE in TCE DNAPL

Bi-component partitioning calculations have been used to predict the nature of occurrence of cDCE within the TCE DNAPL source. Calculated profiles (Fig. 10) are illustrated using the mid-elevation DNAPL-contaminated section of core ST79 data discussed in Fig. 9c. For each observed soil sample composition, a check was made to establish DNAPL presence using the summed soil concentrations to threshold ratio approach of Kueper et al. (2003). If present, a least root-mean-square error DNAPL composition (with conservation of mass) was iteratively determined that assumed a bi-component cDCE–TCE DNAPL (omitting negligible VC) ideally dissolving according to Raoult's law with equilibrium (independent component) K_d partitioning. Calculations assumed similar parameters to the earlier AM f_{oc} -based TCE threshold partitioning calculations with additional parameters for cDCE: K_{oc} 49 L/kg (Chu and Chan, 2000); Solubility 60 mmol (5820 mg/L) (Ramsburg et al., 2010). Whilst recognising the partitioning assumptions are simplified (see, for example, Ramsburg et al. (2010)), the method does provide a quantitative starting point estimate of the allocation of the bulk soils multi-component concentration data between phases (Fig. 10).

Fig. 10a predicts, as expected, the actual DNAPL composition in ST79 is predominantly comprised of TCE whose saturation profile is eclipsed by the near identical total DNAPL S_n field data. Saturations of cDCE exhibited a subdued similar trend reaching a maximum S_n of 0.27% around the uppermost surface of the DNAPL. This is consistent with the aforementioned increase in cDCE at this location (c. 35.8 m) of c. 2–300 mg/kg and is equivalent to a S_n of 0.1 to 0.2% (compared to data points below in the trace DNAPL zone that have a calculated S_n of 0.08%). These saturation values for cDCE are indicative of the quantity of cDCE accumulating (or transiently stored and exchanged) in the TCE DNAPL.

Calculated mole fractions within the DNAPL, X_{cDCE}^n (distinct from X_{cDCE} within the bulk soil sample) shown in Fig. 10c exhibit some variability within the DNAPL, but are generally below 0.05. In the uppermost high residual-pooled DNAPL (Fig. 10c at >35.7 m), there is a trend of increased X_{cDCE}^n predicted towards the DNAPL interface rising from 0.01 to 0.04 over the 0.3 m DNAPL thickness. This trend is ascribed to increased cDCE partitioning nearer to the upper DNAPL interface facilitated by proximity to dechlorination product fluxes in the overlying aqueous-phase plume and lowest DNAPL saturations allowing greatest aqueous-phase permeability. The calculated X_{cDCE}^n of 0.04 in the uppermost DNAPL compares very favourably with the laboratory-theoretical predictions of laboratory partitioning of dechlorination products into DNAPL of Ramsburg et al. (2010) (they provide partitioning values for cDCE into PCE and VC partitioning to TCE).

The threshold mass determined for each component (Fig. 10b), that equates to the mass partitioned to aqueous and sorbed phases and the threshold for multicomponent cDCE–TCE DNAPL existence, is largely driven by the iterated DNAPL mole fraction that controls the effective solubility partitioning to the aqueous phase. Due to its predominance in the DNAPL, the predicted TCE threshold under multicomponent conditions (with cDCE) is only marginally different from the shown TCE-only threshold (earlier AM–606 mg/kg value). This endorses the approach used earlier to predict DNAPL presence from the TCE data alone. Due to the dependence of thresholds on DNAPL mole fractions, thresholds for cDCE are predicted to be quite variable under the multicomponent conditions as it mole fractions range over c. 0.01 to 0.05 leading to thresholds for cDCE ranging from 20 to 80 mg/kg. These values are low as the DNAPL occurrence is predominantly driven by TCE occurrence. For reference, calculated thresholds for cDCE occurrence alone are higher than for TCE, due to its higher solubility with values

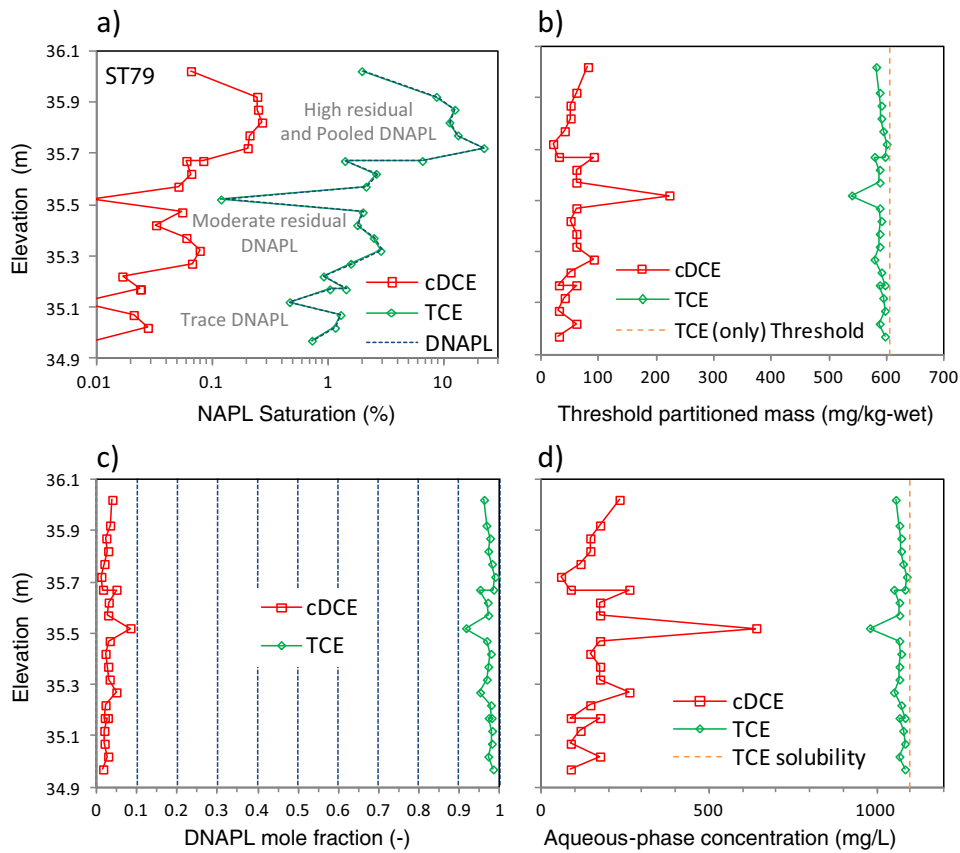


Fig. 10. Equilibrium partitioning—Raoult's law analogue predicted cDCE and TCE profiles within the mid-elevation DNAPL-contaminated section of core ST79 (Transect 1) calculated from observed pre-baseline ST79 soil samples: (a) cDCE and TCE component and DNAPL pore-space saturations (the latter two profiles eclipse each other); (b) equilibrium partitioned mass to aqueous and sorbed phases (i.e., the DNAPL threshold concentration); (c) mole fractions within the DNAPL; and (d) aqueous phase concentrations (effective solubilities) with single-component TCE solubility shown for reference.

calculated of 2020 and 1220 mg/kg (wet) for (rather variable) literature solubility values of 5820 and 3500 mg/l respectively (Chu and Chan, 2000; Pankow and Cherry, 1996).

3.7. Dissolution

3.7.1. Dissolution in the up-gradient source area

Dissolution of the discussed high S_n -low K layer at 36 m elevation (Fig. 8) is illustrated in Fig. 11 that compares S_n , K (projected from T2a) and dissolved-phase TCE at T1, the most up-gradient transect monitored. Localised concentrations at or approaching TCE solubility (S^{TCE} , literature: 3.9–4.0 log μM equivalent to 1100–1400 mg l^{-1}) were observed with much of the monitored transect on the non-T4 side of the cell exceeding 10% solubility. The larger peak of (near) S^{TCE} dissolved concentration immediately overlies the high- S_n -low- K zone with a concentrated plume present within the overlying more permeable unit. Up-gradient S_n data were not available and hence length/time-scales over which these concentrations were attained cannot be established. Nevertheless, Fig. 11 provides excellent, high-resolution characterisation of plume concentration variation close to an aged high- S_n -low- K interface. A high-concentration dissolved-phase plume was also present within the high K gravel unit directly beneath the

contaminated low K unit. This plume potentially evolves from that unit, but also may incorporate dissolution from c. 2% saturations present in the deeper profile and DNAPL sources at the mudstone interface. Both of the T1 plume maxima appear from the T2a K data (Fig. 11) to be located within permeable zones indicating at or approaching solubility concentrations are being attained in moderate to high velocity groundwater and may hence deliver significant mass flux.

3.7.2. Dissolution longitudinally through the source zone

Dissolution longitudinally through the source zone is illustrated via comparison of T4 TCE plume concentrations and soil core profile data showing S_n values >1% (Fig. 12). Near S^{TCE} concentrations were very localised and attained by 11 m distance, some 5 m further down gradient than observed on the non-T4 side of the cell (Fig. 11). High concentrations again coincided with peak saturations along the low K layer at 35.5 m elevation (Fig. 12) as well as a shallow >36 m elevation TCE plume that correlated with elevated saturations at 10 and 13 m distance (Figs. 6b, 12). The zone of active dissolution, indicated by increased concentrations along a flowline (see illustrative labelled flowlines in Fig. 12 assuming flow was approximately along T4), generally shifted more up-gradient and became longer with depth suggesting increased rate-limited mass

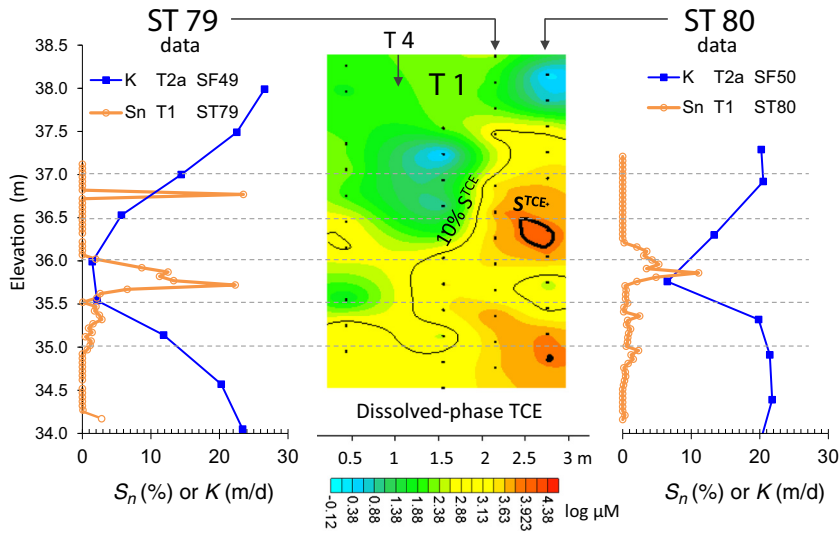


Fig. 11. Comparison of T1 contoured dissolved-phase TCE concentrations at -20 d with DNAPL S_n and K (projected from T2a) profiles for ST79 and ST80 close to the TCE plume hotspots.

transfer. The deeper plume concentration distribution appears indicative of mudstone-related sources and was reasonably expected based on observed upward hydraulic gradients and DNAPL occurrence at this interface (Fig. S2). Only weak dissolved-plume generation was observed from the area underlying the original leakage point (c. 5 m) (in contrast to T1 data on the non-T4 cell side) with the main plume generation over the 6 to 13 m interval. This observation is consistent with continual preferential dissolution of more up-gradient DNAPL and gradual down-gradient shift of the source zone centre of mass and associated mass transfer zones over time.

3.7.3. Dissolution in the down-gradient source area

Cross-cell dissolved-plume monitoring at T2 (Fig. 13) markedly contrasted with the T1 transect 6 m up-gradient (Fig. 11). On the non-T4 cell side, separate plumes above and below the 35.5 m low K layer were still discernible in T2a, however, the high-concentration plume cores observed in T1

were diluted. More elevated concentrations were present at depth on the T4 cell side (in contrast to T1) and correlated with the high DNAPL saturations shown. Although elevated concentrations emanated from just above the 30% S_n in T2a, S^{TCE} concentrations were only encountered towards the lower left side of the transect (SF44) according with the (likely installation induced) mobilised DNAPL in these MLS points. Despite concentrations being high, associated mass fluxes were low as a consequence of the low K (Fig. 13; Cai et al., 2012). T2b data (Fig. 13 inset) indicate increased concentrations over T2a (c. 1 m up-gradient) that could not be fully explained by inter-laboratory analytical variability. Observed concentration increases can be explained by: the correlation of high concentrations with S_n (Fig. 13); T4 longitudinal plume data exhibiting rapid concentration increases around T2; and, literature laboratory studies that show mass transfer to solubility concentrations are attainable in the presence of low S_n over short (several centimetre) length-scales (for

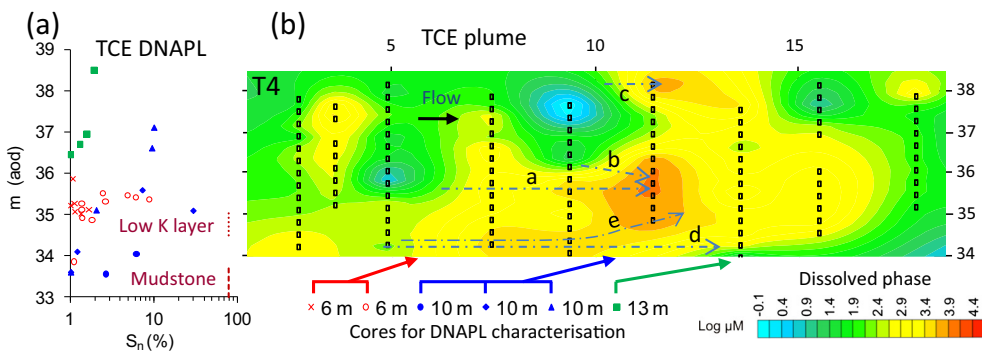


Fig. 12. Comparison of (a) TCE DNAPL saturation depth profiles (for $S_n > 1\%$) at 6, 10 and 13 m along T4 with (b) -49 d baseline T4 dissolved TCE plume data with hypothetical flowlines (a–e) discussed in the text illustrated. The legend for plot (a) is located below plot (b) and indicates the distances along transect T4 from which cores for plot (a) were obtained. Elevations for both plots are identical facilitating data comparison at similar elevations.

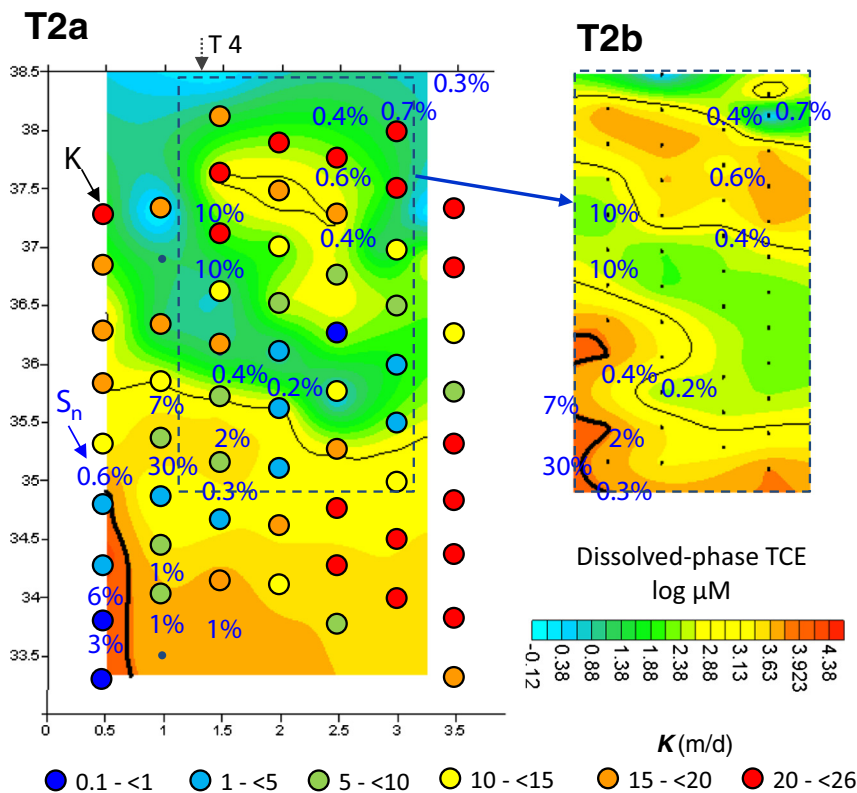


Fig. 13. Comparison of T2a contoured dissolved-phase TCE concentrations at -25 days with K (estimated via MLS point falling head tests) and DNAPL percent S_n data (indicated for $S_n > 0.2\%$) with inset showing T2b dissolved-phase TCE concentrations at -49 days.

example, Imhoff et al. (1994)). Elevated concentrations at 37–38 m in T2b occur in very permeable shallow zones (Fig. 13) and suggest significant mass flux was present close to the water table.

3.7.4. Dissolution mass transfer lengths

Neglecting initially the influence of TCE dechlorination (Section 3.7.5), mass transfer lengths to achieve (near) TCE solubility concentrations indicated by T4 (Fig. 12) and T2a and T2b together (Fig. 13) vary as may be anticipated for this heterogeneous (K and S_n) source zone. Hypothetical flowlines (a – e) are shown in Fig. 12 that assume flow along T4 and trace lines of significant concentration increase. Flowline a along the 35.5 m horizon where saturations may reach 5–30% appeared to require 5 m for a 2 orders of magnitude concentration rise to near solubility. A tentative velocity of 1 m d^{-1} based on T4 bromide data a contact time of 5 d is estimated. Such time and length scales are long compared to those of hours and centimetre to decimetre observed where moderate residual saturations are homogeneously distributed (Imhoff et al., 1994; Rivett and Feenstra, 2005). Alternative flowlines with more rapid concentration increases to (near) TCE solubility may be envisaged in Fig. 12 such as flowlines b and c . The fastest bromide breakthrough velocity observed at the T2a–T4 intersect occurred just above the mudstone interface (Fig. 3) and suggests velocities along flowlines d and e may be around 3 m d^{-1} with contact times of 1–2 d. The plume configuration

at depth is suggestive of dissolving DNAPL at the mudstone interface with anticipated contributions from the mudstone secondary source zone as gradients across the aquitard are upward (Dearden et al., 2013). Moderate to long contact lengths to reach solubility are not that unreasonable based on the observed source zone architecture where the majority of DNAPL mass occupies a small proportion of the source zone area in discrete horizons (Figs. 5.6).

3.7.5. Biodegradation influence upon dissolution

The above said, it was evident that attainment of TCE solubility concentrations was influenced by TCE biotic dechlorination. Hence, the above mass transfer lengths should be regarded as upper-bound (over) estimates. T4 plume data in Fig. 14 demonstrate significant dechlorination product increases, in particular for cDCE over the 2 m interval at 10 to 12 m distance. Plotting 'total ethenes' (sum of chlorinated ethenes and ethene) and contouring summed molar concentration equivalent to the molar TCE solubility suggests solubility-equivalent concentrations occur over much of the cell thickness by around 12 m cell distance. There are some quite rapid concentration increases to these high values although high total ethenes concentrations are variously observed up gradient suggestive of flows oblique to T4. The increases in TCE, dechlorination products and total ethenes concentrations over the above interval confirm biotic dechlorination reactions are occurring within the DNAPL source zone.

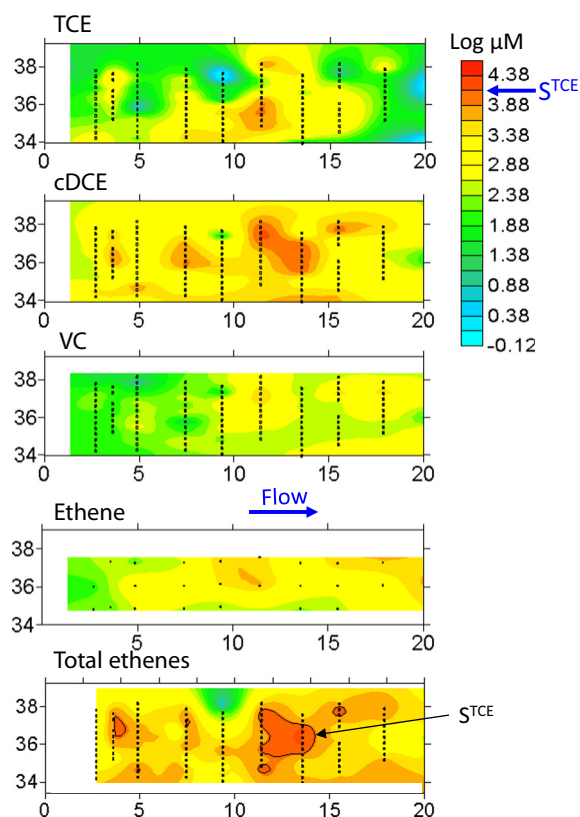


Fig. 14. T4 transect dissolved plume baseline data at -49 d (-20 d for ethene) (flow left to right).

Some limited dissolved-phase over-saturation by degradation products generating above equivalent TCE solubility in the total ethenes plume (at 12–15 m) is potentially indicative of disequilibrium between the DNAPL and the aqueous-phase plume (Serralde et al., 2008) and or biologically-enhanced dissolution (Glover et al., 2007).

3.8. Dissolved-phase plume observations

Orthogonal plume transect depictions in Fig. 15 illustrate the spatial heterogeneity of the plumes emergent from the DNAPL source zone. Due to TCE dechlorination to cDCE and elevated S_n and TCE concentration co-occurrence, increased TCE plume concentrations are indicative of the locality of persistent DNAPL. Dechlorination to cDCE and locally to VC is significant through the source area and immediate down gradient area. Dechlorination occurred cross cell although this was less evident in the permeable gravels overlying the mudstone on the non-T4 cell side where elevated TCE relative to cDCE occurred in both T1 and T2b transects. Geostatistical contaminant flux analysis by Cai et al. (2012) on the T2a data has confirmed that the shallower aquifer conveys the majority of cDCE through T2 and the deep gravel the majority of TCE during the baseline period. This is due to the dominance of the permeability term (Darcy flux). Their analysis truncates at 37.4 m elevation and Fig. 13 suggests significant mass fluxes in shallower and contaminated permeable units transmitting

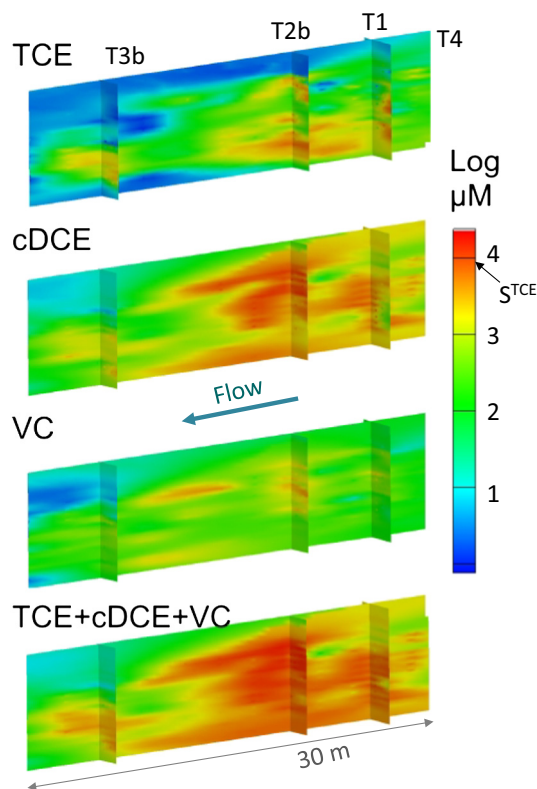


Fig. 15. Dissolved-phase plume baseline data at -49 d obtained from Transects T1, T2b, T3b and T4 (flow right to left).

flow during the baseline period were potentially missed. Although more permeable units provide a significant opportunity to bypass persistent DNAPL zones, Figs. 11 and 13 both support significant mass transfer was still maintained into these high groundwater flux units.

Down-gradient portions of the T4 total chloroethenes plume (Fig. 15) (and total ethenes plume in Fig. 14) reveal, surprisingly, that mid-cell solubility concentrations were not maintained down gradient. The total chloroethenes plume exhibited an order of magnitude concentration decline in T4 at 20 m distance suggesting significant concentration dilution was occurring through dispersive mixing of contaminated and less contaminated groundwater. Certainly some T4 concentration variability, increases and decreases, was caused by oblique flows to T4. Importantly, the discrete TCE peak concentration at 25 m (Fig. 15) coincided with a similar bromide maximum in the 6 d tracer snapshot and is ascribed to plumes moving through the permeable gravels at depth that cross-cuts from the cell side lateral to T4 at T1 and T2 into the T4 transect by T3. This preferential flow line through the cell was relatively TCE rich (high concentrations at 25 m and lower right of T1 and T2 in Fig. 15). TCE persistence was ascribed to the decreased timeframes for biotic dechlorination occurrence within the permeable gravels.

Accounting for the large concentration decline along the cell length has not been fully resolved, but is anticipated to relate to a combination of increased hydraulic gradients at T3 compared to T2, dominance of flows and contaminant fluxes from the more permeable gravel zone, possible convergence of flow

from adjacent horizons (overlying aquifer and underlying mudstone aquitard) into these gravels enhanced by the extraction well withdrawals, accompanying dilution and limited mass transport into the gravels of the high concentration dissolved-phase plumes advecting or diffusing from less permeable units. Additionally, reaction-based contributions to the concentration declines (that would require supporting biogeochemical, compound specific isotope analysis methods and molecular biological tool approaches to elucidate) may include abiotic reactions with, for example, iron phases as well as direct biodegradation of the less chlorinated ethenes and ethene/ethane to CO₂ (Abe et al., 2009; Damgaard et al., 2013). Although cell conditions were generally anaerobic, we note entry of oxygenated rainfall water did infiltrate the upper portions of the cell aquifer during the baseline period and that very low oxygen concentrations, below 0.02–0.1 mg l⁻¹ (below our detection limit), may cause sustained aerobic oxidation of VC to CO₂ (Gossett, 2010).

3.9. Mass flux

Detailed assessment of mass flux was a primary remit of Project SABRE (Cai et al., 2012) and hence summary comments are made to provide some quantitative context to our dissolution discussion. We draw upon both the T2a flux analysis of Cai et al. (2012) and the cell extraction well flux data. The latter measure the cell total effluent and provide an important metric of overall source dissolution and may be used to back calculate average baseline period concentrations in the extracted groundwater. We also calculate a similar average from Cai et al.'s best estimates of baseline mass flux through T2a (Supplementary Data, Table S1). The cell effluent during the baseline contained 25.1% TCE, 65.3% cDCE, 7.4% VC and 2.1% ethene yielding a calculated baseline average concentration of TCE of 958 µmol (2.98 log µmol, 126 mg/l), cDCE of 2491 µmol (3.40 log µmol, 242 mg/l) and total ethenes of 3813 µmol (3.58 log µmol). The TCE average is equivalent to 11% TCE solubility, however, this is an underestimate of the true dissolution rate due to TCE dechlorination occurrence in the cell. The total ethenes concentration, assuming components measured arise from dechlorination of TCE within the cell, is equivalent to 45% TCE solubility and is regarded as our preferred metric of overall source zone dissolution due to the integrative nature of the cell extraction well sample.

The average log µmol individual compound values compare very favourably with T3b data close to the extraction well (Fig. 15) and suggests that most of the mass flux there is being transmitted, even converging, through the mid to lower elevations of T3 within the permeable horizons overlying the mudstone (Fig. 2; also Fig. 16d of Chambers et al. (2010)). The cell extraction well data indicate that the dissolved-phase mass discharging from the source zone would amount to 102 kg per annum of TCE and 314 kg per annum of total ethenes that as TCE equivalent would amount to 406 kg per annum depletion of the source zone monitored. Hence, although an old source zone, its mass depletion across the 4 m by 4 m cross section of aquifer monitored by the cell still amounts to some 0.4 t (tonne) per annum. This is a significant flux considering the source zone is no longer ganglia-dominated and illustrates that the dissolution of a layer/pool-dominated source zone may still be very significant. Based upon the anticipated exponential

decline of DNAPL source zone mass fluxes this annual removal appears a high proportion of the median estimate of source zone mass of 0.9 t and likely suggests the actual source mass may indeed be larger. Even assuming a simple constant 0.4 t per annum dissolution over 20 to 45 years calculates an initial source mass within the monitored streamtube of some 8 to 18 t of DNAPL that would amount to a mean S_n of 10–20% for a nominal 15 m source zone path length. Such saturations are not unreasonable and the masses involved are commensurate with calculations of the wider site source and plume mass by site consultants. Those calculations endorse that the present assessment is of a highly depleted source zone exhibiting a character much removed from its original spill condition.

The mass fluxes calculated by Cai et al. (2012) yield comparable relative percent values to the above (with slightly greater TCE as may be anticipated for the T2a location), but calculate seemingly high average concentrations with a total ethenes concentration of 7078 µmol (3.89 log µmol) equivalent to 93% TCE solubility. This appears unlikely based on the plume concentration observations (Supplementary Material, Table S1). The calculated nodal water flux of Cai et al. was varied spatially across T2a in proportion to the observed *K* with the overall flux matched to the cell extraction rate. We assume the high estimate most likely relates to high concentrations being assigned over too great an area and, or low concentrations assigned over too small an area compared to reality. Whilst agreeing elevated concentrations are prevalent in T2 compared to T3 transects, the mass flux should not exceed that encountered in the cell extraction well unless dilution water influence down gradient of T2a is not being recognised. The latter may be in part true as the down gradient plume concentration distributions monitored have appearances of being diluted (Figs. 14, 15).

Dilution could arise from dispersive mixing, clean recharge water entering the cell down-gradient of T2 (possible during the baseline period), up-coning of less contaminated groundwater from the mudstone in proximity to the extraction well (gradients (0.02) are naturally upward per Dearden et al. (2013)) and low concentration water fluxes through T2 being underestimated. Most of the mass fluxes calculated are dominated by mass transport through the permeable zones (Cai et al., 2012) and as such small errors in concentration assignment may be magnified. Whilst data presented by ourselves and others from T2a and T2b show reasonably high resolution of contamination in the permeable units, Figs. 11 and 13 both suggest spatial resolution could be improved to better quantify mass fluxes through these zones, particularly the deeper gravel that is continuous through the cell, but also the shallow permeable horizons actively flowing during the baseline. The above illustrates the challenges of making mass flux measurements via MLS fences in spatially heterogeneous source area concentration and *K* environments.

4. Conclusions and relevance

Our study provides important field-scale observations relating to the architecture, persistence and dissolution of an aged DNAPL source zone within a heterogeneous sand and gravel aquifer at a UK industrial site. The observations have been made at high spatial resolution within a controlled flow (cell) environment.

Calculated DNAPL threshold concentrations were sensitive to sorption uncertainty and a range of threshold values were used. A resultant outcome was the challenge to differentiate secondary source zone mass from trace DNAPL source mass. Inferred DNAPL presence in samples above the threshold to $<1\% S_n$ (around 25% of our 451 soil samples), should be treated with caution in the absence of sample-specific sorption and, or hydrophobic dye test data. From a practical perspective it may be useful to expand the definition of secondary source zone mass to include trace DNAPL from which release will also be diffusion controlled.

The majority of the TCE source zone mass occurred within discrete layers (lenses/pools) associated with low permeability features. Most mass, 33–42%, was within the moderate residual saturation (1 to $<10\% S_n$) DNAPL category. The high residual saturation category (10 to $<20\% S_n$) at around 2% occurrence, accounted for nearly 25% of the mass. Pooled DNAPL ($>20\% S_n$) at just 1% occurrence, accounted for some 14%. Old sources elsewhere are expected to evolve similarly as they adopt a more pool/lens- rather than ganglia-dominated architecture. Such localised DNAPL may lead to significant uncertainties in total source zone mass estimates and endorses the need for high resolution site investigation approaches.

Persistent high-saturation DNAPL lenses/pools, although supported by lower permeability layers, still primarily occurred within more permeable overlying units where DNAPL is presumed to have initially migrated. A fairly linear declining S_n trend with increasing distance above the (former) pool base was observed and ascribed to preferred gradual dissolution of the uppermost DNAPL. S_n profiles in the underlying low permeability unit declined much more rapidly (approximately exponentially) and were attributed to limited DNAPL entry initially and subsequent diffusion. From a site management perspective, remediation technologies are required that are able to surgically target this DNAPL sub-architecture.

Gradients of cDCE and TCE mole fractions present in bulk soil sample depth profiles markedly changed at the DNAPL interface and provided confirmation of that interface. Declining cDCE mole fractions into the DNAPL were ascribed to decreased cDCE partitioning with distance from the interface. This was confirmed through bi-component soil-partitioning calculations that estimated the mole fraction of cDCE in the DNAPL, X^n_{cDCE} , increased towards the DNAPL interface, from 0.01 to 0.04 over a 0.3 m thickness of DNAPL studied. This important, high resolution, field-scale observation accords with laboratory predictions (Ramsburg et al., 2010). Similar dechlorination product partitioning into DNAPL solvents should be expected at sites where dechlorination has occurred within the source zone, or up gradient.

DNAPL dissolution yielded a heterogeneous dissolved-phase plume containing orders of magnitude local concentration variation that would be unresolved by standard (1.5 or 3 m screen) monitoring wells. Occurrence of (near) TCE solubility concentrations was relatively localised and coincident with high saturation DNAPL lenses. Length scales over which active dissolution mass transfer occurred were around 1–5 m, but difficult to discern in detail due to local flows potentially being oblique to the monitored longitudinal section plane and significant occurrence of biotic dechlorination of dissolved-phase TCE in the source zone. Allowing for the latter, inferred

that a greater proportion of the dissolved-phase plume was attaining TCE equivalent solubility concentrations. Such complexities are probable at most sites.

The conservative tracer test was informative confirming the continuity of a permeable gravel unit through the source zone. Despite this unit allowing significant DNAPL bypassing opportunity and decreased timeframes for dechlorination, it transmitted a significant proportion of the contaminant flux. This was ascribed to a combination of sustained mass transfer from DNAPL at the underlying gravel–mudstone interface, release from the overlying low permeability contaminated strata and convergence of contaminated groundwater into this conductive unit. Whilst more elaborate tracer tests (for example, partitioning tests) would be beneficial, the utility of conservative tracer tests to enhance flow regime understanding at sites should not be overlooked.

Cell extraction well data, our preferred metric of integrated source zone dissolution, indicated a mean baseline concentration of around 45% TCE solubility (taking into account dechlorination). This corresponds to an annual dissolution of 0.4 tonnes of DNAPL over a 16 m² (cell) cross sectional area of flow. It is significant that a decades-old DNAPL source zone containing much of its mass within localised discrete layers can still yield such high contaminant fluxes. Expected exponential source decline (Chen and Jawitz, 2009), would lead to its projected persistence over decades in the absence of remedial intervention.

There remains a need for further detailed field-scale studies on old DNAPL source zones. These could provide: fully 3-D spatial resolution of a DNAPL source zone; more effective demarcation of the DNAPL and secondary source zones within heterogeneous aquifers; increased spatial resolution of individual pools (2-D longitudinal or fully 3-D); improved methods to estimate field-scale mass transfer; assessment of dechlorination product fate; long-term studies that allow improved field-scale insight into the declining strength of more aged source zones; and, studies of source zones in other geologic media.

Acknowledgements

Project Streamtube was funded by CL:AIRE (www.claire.co.uk) through contributions from English Partnerships (now Homes and Communities Agency), the Welsh Assembly Government and the Environment Agency (for England and Wales). The research was carried out under the umbrella of *Project SABRE* (Source Area BioREmediation) funded by the UK Bioremediation LINK Programme. The authors are grateful to *Project SABRE* for research facilitation, provision of various datasets and numerous technical discussions and particularly the SABRE site owners and their consultants for their generous facilitation of the field research. The reviewers are acknowledged for their very insightful comments. This paper is published with the permission of the Executive Director of the British Geological Survey (NERC).

Appendix A. Supplementary data

Supplementary data to this article can be found online at <http://dx.doi.org/10.1016/j.jconhyd.2014.09.008>.

References

- Abe, Y., Aravena, R., Zopfi, J., Parker, B., Hunkeler, D., 2009. Evaluating the fate of chlorinated ethenes in streambed sediments by combining stable isotope, geochemical and microbial methods. *J. Contam. Hydrol.* 107, 10–21. <http://dx.doi.org/10.1016/j.jconhyd.2009.03.002>.
- Blum, P., Annable, M.D., 2008. Partial source zone removal. *J. Contam. Hydrol.* 102 (1–2), 1–2. <http://dx.doi.org/10.1016/j.jconhyd.2008.09.003>.
- Brooks, M.C., Annable, M.D., Rao, P.S.C., Hatfield, K., Jawitz, J.W., Wise, W.R., Wood, A.L., Enfield, C.G., 2002. Controlled release, blind tests of DNAPL characterization using partitioning tracers. *J. Contam. Hydrol.* 59, 187–210. [http://dx.doi.org/10.1016/S0169-7722\(02\)00057-8](http://dx.doi.org/10.1016/S0169-7722(02)00057-8).
- Brovelli, A., Barry, D.A., Robinson, C., Gerhard, J.I., 2012. Analysis of acidity production during enhanced reductive dechlorination using a simplified reactive transport model. *Adv. Water Resour.* 43, 14–27. <http://dx.doi.org/10.1016/j.advwatres.2012.04.000>.
- Brusseau, M.L., Nelson, N.T., Zhang, Z., Blue, J.E., Rohrer, J., Allen, T., 2007. Source zone characterization of a chlorinated-solvent contaminated Superfund site in Tucson, AZ. *J. Contam. Hydrol.* 90 (1–2), 21–40. <http://dx.doi.org/10.1016/j.jconhyd.2006.09.004>.
- Buss, S., Cunningham, C., Ellis, D., Farrar, I., Gerhard, J., Harkness, M., Hart, A., Houlden, L., Lee, M., Wealthall, G., Wilson, R., Zeeb, P., 2010. Project SABRE (Source Area BioRemediation)—an Overview. SABRE Bulletin 1CL:AIRe, London (http://claire.co.uk/index.php?option=com_resource&view=list&category_id=3&Itemid=61).
- Cai, Z., Wilson, R.D., Lerner, D.N., 2012. Assessing TCE source bioremediation by geostatistical analysis of a flux fence. *Ground Water* 50 (6), 908–917. <http://dx.doi.org/10.1111/j.1745-6584.2012.00916.x>.
- Chambers, J.E., Wilkinson, P.B., Wealthall, G.P., Loke, M.H., Dearden, R.A., Wilson, R.D., Ogilvy, R.D., 2010. Hydrogeophysical imaging of deposit heterogeneity and groundwater chemistry changes during DNAPL source zone bioremediation. *J. Contam. Hydrol.* 118 (1–2), 43–61. <http://dx.doi.org/10.1016/j.jconhyd.2010.07.001>.
- Chen, X., Jawitz, J.W., 2009. Convergence of DNAPL source strength functions with site age. *Environ. Sci. Technol.* 43 (24), 9374–9379. <http://dx.doi.org/10.1021/es902108z>.
- Christ, J.A., Ramsburg, C.A., Pennell, K.D., Abriola, L.M., 2010. Predicting DNAPL mass discharge from pool-dominated source zones. *J. Contam. Hydrol.* 114 (1–4), 18–34. <http://dx.doi.org/10.1016/j.jconhyd.2010.02.005>.
- Chu, W., Chan, K.H., 2000. The prediction of partitioning coefficients for chemicals causing environmental concern. *Sci. Total Environ.* 248 (1), 1–10. [http://dx.doi.org/10.1016/S0048-9697\(99\)00472-6](http://dx.doi.org/10.1016/S0048-9697(99)00472-6).
- Damgaard, I., Bjerg, P.L., Bælum, J., Scheutz, C., Hunkeler, D., Jacobsen, C.S., Tuxen, N., Broholm, M.M., 2013. Identification of chlorinated solvents degradation zones in clay till by high resolution chemical, microbial and compound specific isotope analysis. *J. Contam. Hydrol.* 146, 37–50. <http://dx.doi.org/10.1016/j.jconhyd.2012.11.010>.
- Davis, G.B., Barber, C., Power, T.R., Thierrin, J., Patterson, J.L., Rayner, J.L., Wu, Q., 1999. The variability and intrinsic remediation of a BTEX plume in an anaerobic sulphate rich groundwater. *J. Contam. Hydrol.* 36, 265–290. [http://dx.doi.org/10.1016/S0169-7722\(98\)00148-X](http://dx.doi.org/10.1016/S0169-7722(98)00148-X).
- Dearden, R., Chambers, J., Allen, D., Wealthall, G., 2010a. Site investigation techniques for DNAPL source and plume zone characterisation. SABRE Bulletin 2CL:AIRe, London (http://claire.co.uk/index.php?option=com_resource&view=list&category_id=3&Itemid=61).
- Dearden, R., Wealthall, G.P., Chambers, J.E., Rivett, M.O., 2010b. Forced gradient conservative tracer test in the SABRE research cell. British Geological Survey, Commissioned Report CR/09/054 (Nottingham, UK).
- Dearden, R.A., Noy, D.J., Lelliott, M.R., Wilson, R.D., Wealthall, G.P., 2013. Release of contaminants from a heterogeneously fractured low permeability unit underlying a DNAPL source zone. *J. Contam. Hydrol.* 153, 141–155. <http://dx.doi.org/10.1016/j.jconhyd.2011.05.006>.
- Farrell, D.A., Woodbury, A.D., Sudicky, E.A., Rivett, M.O., 1994. Stochastic and deterministic analysis of dispersion in unsteady flow at the Borden Tracer-Test site, Ontario, Canada. *J. Contam. Hydrol.* 15 (3), 159–185. [http://dx.doi.org/10.1016/0169-7722\(94\)90023-X](http://dx.doi.org/10.1016/0169-7722(94)90023-X).
- Feenstra, S., Mackay, D.M., Cherry, J.A., 1991. A method for assessing residual NAPL based on organic chemical concentrations in soil samples. *Groundw. Monit. Remediat.* 11, 128–136. <http://dx.doi.org/10.1111/j.1745-6592.1991.tb00374.x>.
- Glover, K.J., Munakata-Marr, J., Illangasekare, T.H., 2007. Biologically-enhanced mass transfer of tetrachloroethene from DNAPL in source zones: experimental evaluation and influence of pool morphology. *Environ. Sci. Technol.* 41 (4), 1384–1389. <http://dx.doi.org/10.1021/es060922n>.
- Gossett, J.M., 2010. Sustained aerobic oxidation of vinyl chloride at low oxygen concentrations. *Environ. Sci. Technol.* 44, 1405–1411. <http://dx.doi.org/10.1021/es9033974>.
- Grant, G.P., Gerhard, J.I., 2007. Simulating the dissolution of a complex dense nonaqueous phase liquid source zone: 1. Model to predict interfacial area. *Water Resour. Res.* 43, W12410. <http://dx.doi.org/10.1029/2007WR006038>.
- Guilbeault, M.A., Parker, B.L., Cherry, J.A., 2005. Mass and flux distributions from DNAPL zones in sandy aquifers. *Ground Water* 43 (1), 70–86. <http://dx.doi.org/10.1111/j.1745-6584.2005.tb02287.x>.
- Harkness, M., Fisher, A., 2013. Use of emulsified vegetable oil to support bioremediation of TCE DNAPL in soil columns. *J. Contam. Hydrol.* 151, 16–33. <http://dx.doi.org/10.1016/j.jconhyd.2013.04.002>.
- Hartog, N., Cho, J., Parker, B.L., Annable, M.D., 2010. Characterization of a heterogeneous DNAPL source zone in the Borden aquifer using partitioning and interfacial tracers: residual morphologies and background sorption. *J. Contam. Hydrol.* 115 (1–4), 79–89. <http://dx.doi.org/10.1016/j.jconhyd.2010.04.000>.
- Imhoff, P.T., Jaffé, P.R., Pinder, G.F., 1994. An experimental study of complete dissolution of a nonaqueous phase liquid in saturated porous media. *Water Resour. Res.* 30 (2), 307–320. <http://dx.doi.org/10.1029/93WR02675>.
- Jackson, R.E., Jin, M., 2005. The measurement of DNAPL in low-permeability lenses within alluvial aquifers by partitioning tracers. *Environ. Eng. Geosci.* 11 (4), 405–412. <http://dx.doi.org/10.2113/11.4.405>.
- Johnston, C.D., Davis, G.B., Bastow, T.P., Annable, M.D., Trefry, M.G., Furness, A., Geste, Y., Woodbury, R.J., Rao, P.S., Rhodes, S., 2013. The use of mass depletion-mass flux reduction relationships during pumping to determine source zone mass of a reactive brominated-solvent DNAPL. *J. Contam. Hydrol.* 144, 122–137. <http://dx.doi.org/10.1016/j.jconhyd.2012.11.005>.
- Kueper, B.H., Wealthall, G.P., Smith, J.W.N., Leharne, S.A., Lerner, D.N., 2003. An Illustrated Handbook of DNAPL Transport and Fate in the Subsurface. Environment Agency R&D Publication, Bristol, UK (133, <https://publications.environment-agency.gov.uk/skeleton/publications/ViewPublication.aspx?id=2b09791d-44c1-4101-9832-acf5a967f8f8>).
- Lelliott, M.R., Cave, M.R., Wealthall, G.P., 2008. A structured approach to the measurement of uncertainty in 3D geological models. *Q. J. Eng. Geol. Hydrogeol.* 42 (1), 95–105. <http://dx.doi.org/10.1144/1470-9236/07-081>.
- Lyne, F.A., McLachlan, T., 1949. Contamination of water by trichloroethylene. *Analyst* 74 (882), 513. <http://dx.doi.org/10.1039/AN9497400510>.
- McAndrews, B., Heinze, K., DiGiuseppi, W., 2003. Defining TCE plume source areas using the Membrane Interface Probe (MIP). *Soil Sediment Contam.* 12 (6), 799–813. <http://dx.doi.org/10.1080/1714037716>.
- Meinardus, H.W., Dwarakanath, V., Ewing, J.E., Hirasaki, G.J., Jackson, R.E., Jin, M., Ginn, J.S., Londergan, J.T., Miller, C.A., Pope, G.A., 2002. Performance assessment of NAPL remediation in heterogeneous alluvium. *J. Contam. Hydrol.* 54 (3–4), 173–193. [http://dx.doi.org/10.1016/S0169-7722\(01\)00161-9](http://dx.doi.org/10.1016/S0169-7722(01)00161-9).
- Mercur, J.W., Cohen, R.M., Noel, M.R., 2010. DNAPL site characterization at chlorinated solvent sites. Chapter 8 In: Stroo, H.F., Ward, C.H. (Eds.), *In Situ Remediation of Chlorinated Solvent Plumes*. Springer, New York, pp. 217–228.
- Oostrom, M., Dane, J.H., Wietsma, T.W., 2006. A review of multidimensional, multifluid intermediate-scale experiments: nonaqueous phase liquid dissolution and enhanced remediation. *Vadose Zone J.* 5, 570–598. <http://dx.doi.org/10.2136/vzj2005.0125>.
- Pankow, J.F., Cherry, J.A., 1996. *Dense Chlorinated Solvents and other DNAPLs in Groundwater*. Waterloo Press, Oregon.
- Pankow, J.F., Feenstra, S., Cherry, J.A., Ryan, M.C., 1996. Dense chlorinated solvents in groundwater: background and history of the problem. In: Pankow, J.F., Cherry, J.A. (Eds.), *Dense Chlorinated Solvents and Other DNAPLs in Groundwater*. Waterloo Press, Portland, OR.
- Parker, B.L., Cherry, J.A., Chapman, S.W., Guilbeault, M.A., 2003. Review and analysis of chlorinated solvent dense nonaqueous phase liquid distributions in five sandy aquifers. *Vadose Zone J.* 2, 116–137. <http://dx.doi.org/10.2113/2.2.116>.
- Parker, J.C., Park, E., 2004. Modelling field-scale dense nonaqueous phase liquid dissolution kinetics in heterogeneous aquifers. *Water Resour. Res.* 40, W05109. <http://dx.doi.org/10.1029/2003WR002807>.
- Puigserver, D., Carmona, J.M., Cortés, A., Viladevall, M., Nieto, J.M., Grifoll, M., Vila, J., Parker, B.L., 2012. Subsoil heterogeneities controlling porewater contaminant mass and microbial diversity at a site with a complex pollution history. *J. Contam. Hydrol.* 144, 1–19. <http://dx.doi.org/10.1016/j.jconhyd.2012.10.009>.
- Ramsburg, C.A., Thornton, C., Christ, J.A., 2010. Degradation product partitioning in source zones containing chlorinated ethene dense non-aqueous-phase liquid. *Environ. Sci. Technol.* 44, 9105–9111. <http://dx.doi.org/10.1021/es102536f>.
- Rao, P.S.C., Jawitz, J.W., 2003. Comment on “Steady-state mass transfer from single-component dense non-aqueous phase liquids in uniform flow fields”

- by T. C. Sale and D. B. McWhorter. *Water Resour. Res.* 39 (3), 1068. <http://dx.doi.org/10.1029/2001WR000599>.
- Riley, R.G., Szecsody, J.E., Mitroshkov, A.V., Brown, C.F., 2006. Desorption behavior of trichloroethene and tetrachloroethene in U.S. Department of Energy Savannah River Site unconfined aquifer sediments. Pacific Northwest National Laboratory (PNNL) report 15884 (http://www.pnl.gov/main/publications/external/technical_reports/PNNL-15884.pdf).
- Rivett, M.O., Allen-King, R.M., 2003. A controlled field experiment on groundwater contamination by a multicomponent DNAPL: dissolved-plume retardation. *J. Contam. Hydrol.* 66, 117–146. [http://dx.doi.org/10.1016/S0169-7722\(03\)00006-8](http://dx.doi.org/10.1016/S0169-7722(03)00006-8).
- Rivett, M.O., Feenstra, S., 2005. Dissolution of an emplaced source of DNAPL in a natural aquifer setting. *Environ. Sci. Technol.* 39, 447–455. <http://dx.doi.org/10.1021/es040016f>.
- Rivett, M.O., Lerner, D.N., Lloyd, J.W., Clark, L., 1990. Organic contamination of the Birmingham aquifer. *J. Hydrol.* 113, 307–323. [http://dx.doi.org/10.1016/0022-1694\(90\)90181-V](http://dx.doi.org/10.1016/0022-1694(90)90181-V).
- Rivett, M.O., Feenstra, S., Cherry, J.A., 2001. A controlled field experiment on groundwater contamination by a multicomponent DNAPL: creation of the emplaced-source and overview of dissolved plume development. *J. Contam. Hydrol.* 49, 111–149. [http://dx.doi.org/10.1016/S0169-7722\(00\)00191-1](http://dx.doi.org/10.1016/S0169-7722(00)00191-1).
- Rivett, M.O., Feenstra, S., Clark, L., 2006. Lyne and McLachlan (1949): influence of the first publication on groundwater contamination by trichloroethene. *Environ. Forensic* 7 (4), 313–323. <http://dx.doi.org/10.1080/15275920600996180>.
- Rivett, M.O., Dearden, R.A., Wealthall, G.P., 2010. Streamtube Project overview: longitudinal transect assessment of the SABRE Site DNAPL source zone. CL: AIRE Research Bulletin RB 11CL:AIRE, London (http://claire.co.uk/index.php?option=com_resource&view=list&category_id=3&Itemid=61).
- Rivett, M.O., Turner, R.J., Glibbery, P., Cuthbert, M.O., 2012. The legacy of chlorinated solvents in the Birmingham aquifer, UK: observations spanning three decades and the challenge of future urban groundwater development. *J. Contam. Hydrol.* 140–141, 107–123. <http://dx.doi.org/10.1016/j.conhyd.2012.08.006>.
- Rowe, B.L., Toccalino, P.L., Moran, M.J., Zogorski, J.S., Price, C.V., 2007. Occurrence and potential human-health relevance of volatile organic compounds in drinking water from domestic wells in the United States. *Environ. Health Perspect.* 115 (11), 1539–1546. <http://dx.doi.org/10.1289/ehp.10253>.
- Sale, T., Newell, C., 2011. A guide for selecting remedies for subsurface releases of chlorinated solvents. ESTCP Project ER-200530. (http://estcp14cmodel.com/downloads/ESTCP_Decision_Guide_Sale_Newell.pdf).
- Serralde, C., Rivett, M.O., Molson, J.W., 2008. Interaction of multiple in-series DNAPL residual source zones: implications for dissolution, repartitioning and DNAPL mobilization at contaminated industrial sites. GQ07: Securing Groundwater Quality in Urban and Industrial Environments. IAHS Publ. 324, pp. 388–395.
- Seyedabbasi, M.A., Newell, C.J., Adamson, D.T., Sale, T.C., 2012. Relative contribution of DNAPL dissolution and matrix diffusion to the long-term persistence of chlorinated solvent source zones. *J. Contam. Hydrol.* 134–135, 69–81. <http://dx.doi.org/10.1016/j.jconhyd.2012.03.010>.
- Stroo, H.F., Unger, M., Ward, C.H., Kavanaugh, M.C., Vogel, C., Leeson, A., Marqusee, J.A., Smith, B.P., 2003. Remediating chlorinated solvent source zones. *Environ. Sci. Technol.* 37 (11), 224A–230A. <http://dx.doi.org/10.1021/es032488k>.
- US EPA, 2003. National Risk Management Research Laboratory, U.S. Environmental Protection Agency, Cincinnati, Ohio (www.dtic.mil/cgi-bin/GetTRDoc?Location=U2&doc=GetTRDoc.pdf&AD=ADA512081).
- US EPA (U.S. Environmental Protection Agency), 1996. Soil screening guidance: technical background document. EPA/540/R-95/128. (http://www.epa.gov/superfund/health/conmedia/soil/pdfs/part_5.pdf).
- US EPA (U.S. Environmental Protection Agency), 2002. Supplemental guidance for developing soil screening levels for Superfund Sites. EPA OSWER 9355.4-24. ([http://www.epa.gov/superfund/health/conmedia/soil/#fact with specific link at http://www.epa.gov/superfund/health/conmedia/soil/pdfs/appd_k.pdf](http://www.epa.gov/superfund/health/conmedia/soil/#fact%20with%20specific%20link%20to%20http://www.epa.gov/superfund/health/conmedia/soil/pdfs/appd_k.pdf)).
- Wang, F., Annable, M.D., Jawitz, J.W., 2013a. Field-scale prediction of enhanced DNAPL dissolution based on partitioning tracers. *J. Contam. Hydrol.* 152, 147–158. <http://dx.doi.org/10.1016/j.jconhyd.2013.07.001>.
- Wang, G., Allen-King, R.M., Choung, S., Feenstra, S., Watson, R., Kominek, M., 2013b. A practical measurement strategy to estimate nonlinear chlorinated solvent sorption in low foc sediments. *Groundw. Monit. Remediat.* 33 (1), 87–96. <http://dx.doi.org/10.1111/j.1745-6592.2012.01413>.
- Wealthall, G., Cave, M., Dearden, R., Zeeb, P., Wilson, R., 2010. Establishing clean-up criteria at the Source Area Bioremediation (SABRE) site: the development of uncertainty-based methods to quantify DNAPL mass removal and flux reduction. Proc. ATV Meeting, Clean-up criteria for groundwater and risk assessment tools, Copenhagen, 2 November 2010 (www.atv-jordgrundvand.dk/Afholdte_moeder/101102moede63/Rapport%2063.pdf).
- White, R.A., Rivett, M.O., Tellam, J.H., 2008. Paleo-roothole facilitated transport of aromatic hydrocarbons through a Holocene clay bed. *Environ. Sci. Technol.* 42 (19), 7118–7124. <http://dx.doi.org/10.1021/es800797u>.
- Zeeb, P., Houlden, L., 2010. Overview of the SABRE field tests. CL:AIRE (Contaminated Land: Applications in Real Environments) SABRE Bulletin 5CL: AIRE. London (http://claire.co.uk/index.php?option=com_resource&view=list&category_id=3&Itemid=61).
- Zhang, C., Yoon, H., Werth, C.J., Valocchi, A.J., Basu, N.B., Jawitz, J.W., 2008. Evaluation of simplified mass transfer models to simulate the impacts of source zone architecture on nonaqueous phase liquid dissolution in heterogeneous porous media. *J. Contam. Hydrol.* 102, 49–60. <http://dx.doi.org/10.1016/j.jconhyd.2008.05.007>.